CO6-1

Radiolabeling of composite natural material chicken eggshell membrane via neutron irradiation 6Li(n,α) 3H reaction

M. Shimizu[1], E. Ohto-Fujita[1], N. Nogawa[2], H. Yoshinaga[3], K. Takamiya[3], A. Enomoto[4], K. Tanoi[5], T. Yamashita[6], and Y. Atomi[1]

[1]*Teikyo University, Advanced Comprehensive Research Organization, Division of Open Innovation*
[2]*Isotope Science Center, The University of Tokyo*
[3]*Institute for Integrated Radiation and Nuclear Science, Kyoto University*
[4]*Isotope Facility, Graduate School of Medicine, The University of Tokyo*
[5]*Isotope Facility for Agricultural Education and Research. Graduate school of Agricultual and Life Sciences, University of Tokyo.*
[6]*Department of dermatology, Graduate School of Medicine, The University of Tokyo*

INTRODUCTION: Chicken eggshell membrane (ESM) has been listed as an excellent wound-healing agent in Chinese pharmacopoeia book entries for 400 years. It is a non-woven fabric composed of fibrous biopolymers that are mainly protein-based and contain a large amount of extracellular matrix such as collagen and proteoglycans, as well as antibacterial proteins, cross-linked by lysyl-oxidase [1]. Recently, proteomic analysis has revealed that it contains more than 400 different proteins. We previously found that hydrolyzed ESM provide young extracellular environment to dermal fibroblast [2] and improved skin elasticity and reduced facial wrinkles when topically applied as cosmetics [3]. Ingestion of this non-woven fabric has been reported to improve pain in knee joints and prevent liver fibrosis and ulcerative colitis in animal experiments. In our previous studies, we have found that eggshell membrane supplements improved skin elasticity, respiratory function, and locomotion (especially balance function) in healthy adults within 8 weeks of taking the supplements [4]. ESMs are secreted by cells in the narrow oviduct of the parent bird and serve as a biomineralization scaffold for eggshell formation and to protect chick embryo from drying and infection. We applied the tritium labeling of organic compounds via the 6Li(n,α)3H reaction, which has been used for radiolabeling of natural products that are difficult to synthesize and for tissue distribution in individuals, to ESM and conducted pilot experiments to determine whether ingested ESM are indeed digested and absorbed and distributed to various tissues. The labeled eggshell membrane was orally administered to mice and was digested and absorbed. The radioactivity derived from the labeled ESM was detected in blood 2 hours after administration, peaking 6 hours later, and was also detected in almost all tissues [5]. However, in the previous irradiation experiment with JRR-4 (3.5 MW, 20 min), many parts of the sample were scorched, and the optimization of the eggshell membrane to lithium carbonate ratio and irradiation conditions remained an issue. The Kyoto University furnace is beneficial for irradiating protein samples because its low power output does not raise the sample temperature during irradiation.

****

EXPERIMENTS: ESM (nano-sized extra-fine form, Almado Inc.) + Li_2CO_3 (65:35 by weight) and lysozyme or ovotransferrin (one of the major proteins of ESM) + Li_2CO_3 (65:35 by weight) sealed in quartz glass were irradiated under milder conditions (Pn-2, 1 MW, 70 min). After irradiation, samples were transferred to The University of Tokyo for biochemical and in vivo study.

****

RESULTS:【R4193 tritium-labeled ESM (2022) (research update)】Mice were orally fed once with tritium-labeled ESM for detailed verification of the pharmacokinetics and cellular uptake. The tritium-labeled eggshell membrane was mixed with medical jelly and given to B6 mice as a single oral dose as a supplement and kept individually in metabolic cages. Then, 0.5, 2, 5, 24, 48, and 72 hours later, blood was drawn from an abdominal vein under anesthesia, and PBS was perfused through the

heart to drain blood from the tissues. Approximately 30 different organs were isolated (n=4 each time). A tritium count study in serum revealed a peak at about 5 hours, like the results of the previous pilot experiment [4]. Continuous study is ongoing to quantify the distributed radioactivity to more than 20 tissues using a liquid scintillation counter. One of the tissue (liver) specimens was prepared for histochemical analysis using a cryostat, and the ^{3}H distribution was analyzed using an imaging analyzer. A preliminary experiment showed that the detection of radioactivity was not successful after 7 months of exposure to the image plate. Thus, multiple administrations of rebelled eggshell membranes are necessary for this purpose.

【R5010 tritium-labeled ESM and lysozyme (2023) study (to be performed)】The chemical integrity of the protein after Pn-2 irradiation and the peptide size after digestion and absorption into the serum and mouse tissues will be determined using SDS-PAGE and peptide gel. Using cell line, uptake of labeled protein and secretion of ECM (decorin, type III collagen, MMP2) will determine the biological activity of the irradiated protein sample.

****

REFERENCES:

[1] M. Shimizu *et al.*, The journal of Japan Mibyou Association, **30** (2024) 23-26.
[2] E. Ohto-Fujita *et al.*, Cell Tissue Res., **345** (2011) 177-190.
[3] E. Ohto-Fujita *et al.*, Cell Tissue Res., **376** (2019)123-135.
[4] E. Ohto-Fujita *et al.*, Journal of Fiber Science and Technology, **77** (2021) 258-265 (2021) 115-120.
[5] E. Ohto-Fujita *et al.*, Journal of Fiber Science and Technology, **77** (2021) 182-187.

CO6-2

Interaction between Mint3 and FIH-1 involved in hypoxia stress responses

R. Maeda, S. Nagatoishi[1], K. Tsumoto[1], K. Morishima[2], R. Inoue[2], M. Sugiyama[2] and M. Hoshino
Graduate School of Pharmaceutical Sciences, Kyoto University
[1]*Institute of Medical Science, the University of Tokyo*
[2]*Institute for Integrated Radiation and Nuclear Science, Kyoto University*

INTRODUCTION: Oxygen is essential for many organisms to produce ATP efficiently from nutrients in food. Temporal or local drop of oxygen level induces cells to change the metabolic pathway. This is called stress responses, which are mainly triggered by hypoxia inducible transcriptional factors (HIFs). Under the normal oxygen conditions, transcriptional activities of HIFs in the cells are inhibited by the factor inhibiting HIF-1 (FIH-1). Munc-18 interacting protein 3 (Mint3) is recently found to activate the hypoxia responses by binding and inhibiting the activity of FIH-1 in these cells under the normal oxygen conditions [1]. Although the N-terminal 214 residues (Mint3NT) are found to be necessary for the interaction with FIH-1 to inhibit its activity, little is known about inhibitory mechanisms. We investigated the interaction between Mint3NT and FIH-1 by small-angle X-ray scattering, analytical ultracentrifugation, and solution-state NMR.

EXPERIMENTS: The N-terminal fragment proteins of Mint3 (Mint3NT) and full-length FIH-1 were expressed by *E. coli* BL21 strains. The proteins were expressed in bacteria grown in LB-broth and ^{15}N-enriched M9 minimal medium to produce unlabeled and ^{15}N-labeled proteins, respectively. NMR experiments were performed on a Bruker Avance 600 spectrometer equipped with a triple-resonance probe. A typical ^{1}H-^{15}N HSQC experiments were performed at protein concentration of 50 μM dissolved in 20 mM sodium phosphate (pH 7.3) and 10% D_2O.

RESULTS: We measured the ^{1}H-^{15}N HSQC spectrum of Mint3NT, and found that the dispersion of resonance peaks was very poor particularly along the ^{1}H-axis, suggesting the absence of strong hydrogen-bonding interactions. We prepared several fragment proteins of 214-residue protein Mint3NT. The superposition of the spectra separately recorded with the fragment proteins were found to be essentially the same as that of the whole protein, suggesting that the absence of significant interaction between the N- and C-terminal regions of Mint3NT. With these fragment proteins of Mint3NT, we unambiguously assigned more than 95% peaks by analyzing several triple-resonance spectra. The titration experiment of ^{15}N-labled Mint3NT by unlabeled FIH-1 revealed that the peak intensities for many residues were remarkably decreased in a concentration dependent manner. By mapping the change in the peak intensity along the primary structure of the protein, we found that a broad range of residues were significantly affected by the addition of unlabeled FIH-1, suggesting the involvement of these residues in the interaction between Mint3NT and FIH-1.

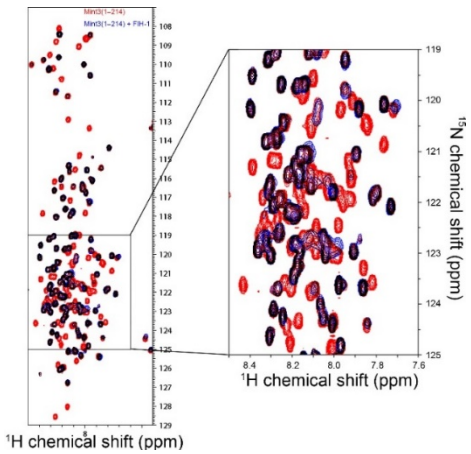

Fig. 1. ^{1}H,^{15}N-HSQC spectra of ^{15}N-Mint3NT in the absence (red) and presence (blue) of equimolar amount of unlabeled FIH-1. Peaks significantly decreased in intensity are shown in red.

REFERENCES:
[1] Sakamoto *et al.,* Mol. Cell Biol., **34** (2014) 30-42.
[2] Ten *et al.,* J. Biol. Chem. **297** (2021) 101304.

CO6-3

Integrated structural analysis of clock protein complex using analyatical ultracentrifugation and small-angle X-ray scattering

K. Morishima, M. Shimizu, A. Okuda, N. Sato, R. Inoue, and M. Sugiyama

Institute for Integrated Radiation and Nuclear Science, Kyoto University

INTRODUCTION:

Cyanobacteria has one of the simplest circadian clocks which consists of only three clock proteins (KaiA, KaiB, and KaiC) and adenosine triphosphate (ATP). The three clock proteins undergo an association-dissociation cycle correlated with phosphorylation-dephosphorylation oscillation of KaiC with 24 h-period. In the circadian cycle, the three types of complexes appear; KaiA-KaiC (AC), KaiB-KaiC (BC), and KaiA-KaiB-KaiC (ABC) complexes. Among them, AC complex has a significant function for the circadian cycle, that is, the promotion of phosphorylation of KaiC. To understand the molecular mechanism of the phosphorylation, it is necessary to reveal the three-dimensional structure of AC complex. However, there are obstacles on the structural analysis of AC complex.

EXPERIMENTS:

In this study, we utilized the small-angle X-ray and neutron scattering (SAXS and SANS; collectively called SAS) to analyze its solution structure. The SAS profile purely from AC complex is essential for building its structural model. Nevertheless, AC complex cannot be predominantly purified with a general separation method such as size exclusion chromatography due to the fast association-dissociation equilibrium, KaiA + KaiC ↔ AC complex. To overcome this problematic situation, we applied to the integrated approach with analytical ultracentrifugation (AUC) and SAS, namely AUC-SAS [1,2].

RESULTS: AUC offered the concentration distribution of KaiA, KaiC, AC complex, and their aggregates in the mix solution of KaiA and KaiC. The experimental SAXS profile of the mix solution (open circles in Fig.1) was given as the ensemble-average of these components. Therefore, we derived the SAXS profile of AC complex from the experimental profile with AUC-SAS as shown in Fig.1. (Here, the SAXS profiles of KaiA and KaiC were obtained by the individual measurements.) Finally, we obtained the candidate structural model of AC complex through the combination of the SAXS profile and coarse-grained molecular dynamics simulation.

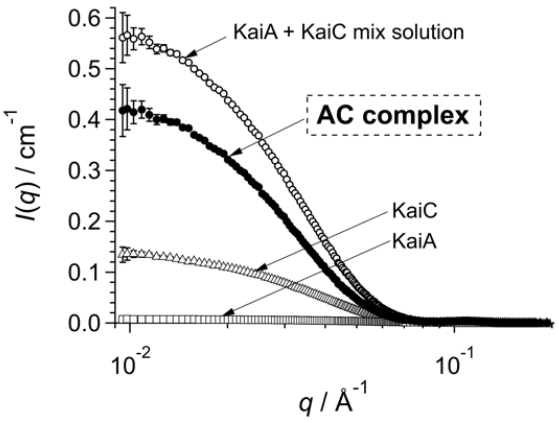

Fig. 1. Open circles, squares, triangles represent the experimental SAXS profiles of the KaiA + KaiC mix solution, KaiA, and KaiC, respectively. Closed circles show the SAXS profiles of AC complex derived with AUC-SAXS-treatment.

REFERENCES:

[1] K. Morishima *et al.,* Commun. Biol., **3** (2020) 294.

[2] K. Morishima *et al.,* J. Appl. Crystallogr., **56** (2023) 624.

CO6-4

Elucidation of the effects of dose rate of radiation on normal and tumor tissues

T. Watanabe[1], Y. Sanada[2], T. Takata[3], G. E.Sato[4], M. Yoshimura[4], Y. Sakurai[3], H. Tanaka[3], M. Suzuki[1], T. Mizowaki[4]

Institute for Integrated Radiation and Nuclear Science, Kyoto University
[1]Particle Radiation Oncology, Particle Radiation Oncology Research Center
[2]Particle Radiation Medical Physics, Particle Radiation Oncology Research Center
[3]Division of Radiation Life Science
[4]Radiation Oncology and Image-Applied Therapy, Faculty of Medicine, Kyoto University

INTRODUCTION: Radiation with different dose rates is known to have different effects on normal tissues [1]. On the other hand, the effect of dose rate on the antitumor effect is minor, and a higher dose rate may improve the therapeutic efficacy ratio of radiation [2]. The purpose of this study is to ascertain whether the dose rate alters the effects of various normal tissues. In addition, experiments were conducted to see if the antitumor effect of radiation could be differentiated by differences in dose rate, which had previously been equivalent, by using drugs that affect the anti-tumor effect of radiation in combination.
****

EXPERIMENTS: A mouse subcutaneous transplantation model of mouse-derived squamous cell carcinoma cells (SCC7) was used for experiments in C3H mice under the lower limb skin. The differences in the effects of irradiation with electron beams with high dose rates and X-rays with low dose rates on normal and tumor tissues were investigated. The irradiation area was limited to the lower extremities, the remaining area was shielded, and the tumor tissue was irradiated with a single 14 Gy dose. Changes in the skin after irradiation were observed over time in the X-irradiated group and the high-dose-rate electron irradiated group. SCR, which is the inhibitor of non-homologous end joining mechanism in DNA reapair, was used as agents affecting the DNA-repair mechanism after irradiation [3]. SCR was each administered 1 hour before irradiation, and tumor tissue was irradiated to confirm tumor size over time.
****

RESULTS: The skin in the irradiated also showed obvious alopecia, wet desquamation and dermatitis in the X-ray group, whereas the skin in the high-dose-rate electron beam group showed only slight alopecia, no wet desquamation, and no dermatitis. Compared to the X-ray group, the high-dose rate electron beam group showed the same tumor control under the same irradiation dose. When X-rays were irradiated after preadministration of SCR to subcutaneous tumors in mice, the anti-tumor effect of X-rays was sensitized. However, contrary to our expectation, the sensitization effect of SCR was not enhanced in the high-dose rate electron beam irradiation compared to the X-ray group. When SCR was preadministered to subcutaneous tumors of mice and then irradiated with high-dose-rate electron beams, the effect to the normal tissue including the surrounding skin was also similar to that in X-ray group.
****

REFERENCES:
[1] B. Lin *et al.,* Front Oncol., **11** (2021) 644400.
[2] E. Konradsson *et al.,* Advances in Ra-diation Oncology., **7** (2022) 101011.
[3] M. Srivastava *et al.,* Cell., **151** (2012) 1474-87.

CO6-5

Design, Synthesis, and BNCT Effect of Macrocyclic Polyamine-type Boron Carriers for BNCT

S. Aoki[1,2], H. Ueda[3], W. Yoshida[1], M. Suzuki[3], Tanaka, T.[1,4] S Masunaga[3], N. Kondo[3], and Y. Sakurai[3]

[1]*Faculty of Pharmaceutical Sciences, Tokyo University of Science*
[2]*Research Institute for Science and Technology, Tokyo University of Science*
[3]*Research Reactor Institute, Kyoto University*
[4]*Faculty of Pharmaceutical Sciences, Okayama University*

INTRODUCTION: Neutron capture therapy using boron-10 (^{10}B) (BNCT) is one of powerful therapies for local tumor control in the treatment of brain tumor, melanoma, and related diseases. We previously designed and synthesized phenylboronic acid-pendant 9-, 12-, and 15-membered macrocyclic amines such as **^{10}B-1a~3a** and their corresponding Zn^{2+} complexes **^{10}B-1b~3b** (Fig. 1) [2], based on high intracellular uptake pendant-cyclen (cyclen = 1,4,7,10-tetraazacyclododecane) in cancer cells. It was reported that the metal-free **^{10}B-1a~3a** are introduced into cancer cells (A549 and HeLa S3 cells) more efficiently than their Zn^{2+} complexes **^{10}B-1b~3b** with considerably high cancer/normal cells selectivity. Besides, it was found that 12- and 15-membered derivatives **^{10}B-2a~3a** exhibit a higher BNCT effect than **^{10}B-1a**, possibly because **^{10}B-2a~3a** form the corresponding Zn^{2+} complexes **^{10}B-2b** & **3b**, which strongly interact with DNA in living cells, resulting in the efficient breakdown of DNA double-strand upon the neutron irradiation.

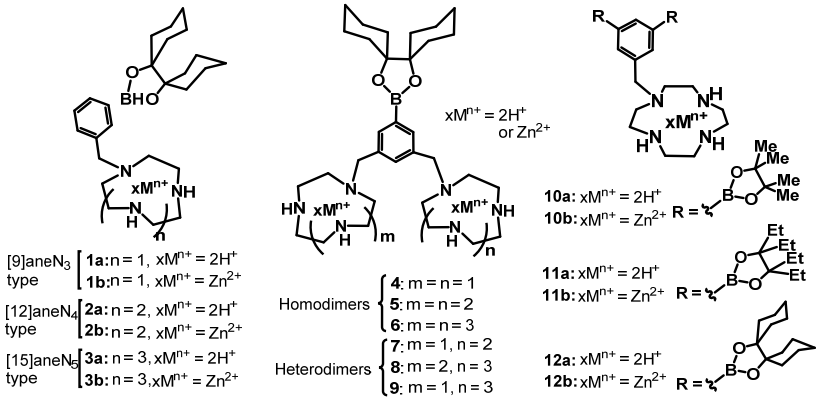

Figure 1. Chemical Structures of Borono Compounds **1**～**12**

Next, we conducted the design and synthesis of dimeric macrocyclic polyamines connected via one phenylboronic acid unit such as **4~6** (homodimers) and **7~9** (heterodimers) and their corresponding Zn^{2+} complexes (Fig. 1), because it was well established that polymeric Zn^{2+} complexes would form more stable complexes with DNA double strand than monomeric Zn^{2+} complexes [3]. However, the intracellular uptake of **4~9** and their Zn^{2+} complexes were lower than monomeric compounds **1~3**, possibly due to their lower hydrophobicity than that of **1~3.**

EXPERIMENTS and RESULTS:

The aforementioned results have prompted us to synthesize monomeric polyamines equipped with two boronic ester units for higher intracellular uptake and BNCT effect and for the observation of these ^{11}B-containing compounds (naturally occurring abundant content) for non-invasive magnetic resonance imaging (MRI) of BNCT agents in living systems. In 2023, **10a~12a** and their corresponding Zn^{2+} complexes **10b~12b** were synthesized and the evaluation of their intracellular uptake and toxicity against cancer cells is now in progress.

REFERENCES:

[1] H. Ueda *et al.,* J. Med. Chem., **64** (2021) 8523-8544.
[2] S. Aoki, E. Kimura, Chem. Rev., **104** (2004) 769-788.
[3] H. Ueda *et al.,* Eur. J. Inorg. Chem., **2022** (2022) e202100949 (24 pages).
[4] S. Aoki *et al.,* In "*Characteristics and Applications of Boron*" 2022, pp 83-105, Charchawal Wongchoosuk, Ed., IntechOpen, Croatia

CO6-6

Small-angle X-ray scattering analysis of nucleosomes containing parasite histones

S. Sato[1], K. Morishima[2], R. Inoue[2], N. Sato[2], M. Dacher[1], N. Horikoshi[1], M. Sugiyama[2], H. Kurumizaka[1]

[1]*Institute for Quantitative Biosciences, The University of Tokyo*
[2]*Institute for Integrated Radiation and Nuclear Science, Kyoto University*

INTRODUCTION: In eukaryotic cells, genomic DNA is organized into chromatin, which plays an essential role not only in tightly packaging DNA into the cell nucleus, but also in dynamically regulating biological events such as gene transcription, DNA repair, and replication. The nucleosome is the structural unit of chromatin, in which 145-147 base-pairs of DNA are wrapped around a histone octamer, containing two molecules each of histone proteins H2A, H2B, H3, and H4. The dynamics of nucleosomes impacts those of chromatin, which is fundamentally composed of the nucleosome array. A large number of unicellular eukaryotes are infectious human parasites, with low sequence identity to human histones. The characteristics of parasite chromatin remained unknown until now. Here, we investigated the structures of the nucleosomes in solution, containing histones from *Plasmodium falciparum*, the parasite responsible for human malaria.

EXPERIMENTS: The nucleosomes were prepared by *in vitro* reconstitution [1]. Recombinant human or parasite histones were mixed with a 145 base-pair DNA fragment containing a strong nucleosome positioning sequence under high salt conditions, followed by a gradual decrease in salt concentration to promote nucleosome formation, and then purification using a method based on polyacrylamide gel electrophoresis [1]. The nucleosomes thus obtained were analyzed by small-angle X-ray scattering (SAXS) under conditions of 50 or 150 mM NaCl concentration, as ionic strength is known to affect nucleosome conformation. SAXS intensity of the buffer solution was measured for background subtraction, using the same conditions and procedure as for the nucleosome samples. SAXS data were collected using a laboratory-based instrument equipped with a high-brilliance point-focused generator of a Cu Ka source. To assess aggregation and dissociation of nucleosome samples, sedimentation velocities were measured by analytical ultracentrifugation [2]. Scattering profiles (one-dimensional intensity data $I(q)$ as a function of magnitude of scattering vector q) of nucleosomes were calculated as aggregated components were removed [2]. Radius of gyrations (R_g) were estimated from the fitting curves of the $I(q)$ data using Guinier plot, as previously described [3].

RESULTS: The R_g of the parasite nucleosome is similar to that of the human nucleosome under conditions of 50 and 150 mM NaCl. DNA detachment from the histone surface of the nucleosome leads to an increase of R_g [3]. Our data suggest that the intact nucleosome containing parasite histones retains a canonical structure under physiological condition of ionic strength, even though the amino acid sequences diverge from those of human histones.

REFERENCES:

[1] T. Kujirai *et al.*, Methods Mol. Biol., **1832** (2018) 3-20.
[2] K. Morishima *et al.*, J. Appl. Crystallogr., **56** (2023) 624-632.
[3] Y. Arimura *et al.*, Sci. Rep., **3** (2013) 3510.

CO6-7

Elucidation of the oligomeric structure and activation mechanism of the small heat shock protein HspB7

K. Iino, M. Ogawa, K. Morishima[1], R. Inoue[1], M. Sugiyama[1] and M. Yohda

Department of Biotechnology and Life Science, Tokyo University of Agriculture and Technology
[1]Institute for Integrated Radiation and Nuclear Science, Kyoto University

INTRODUCTION: Small Heat Shock Proteins (sHSPs) are known to exhibit chaperone function by changing its oligomeric structure [1]. A mammalian sHsp, HspB7, possesses a strong chaperone function to prevent the aggregation of polyQ. We tried to create functional HspB7 and analyze its structure and functional mechanism. However, as the acquisition of functional HspB7 was unsuccessful, we proceeded with a change in the objective. Analysis of the oligomer dissociation mechanism and the structure of the dissociated active state of sHSP has not progressed due to the difficulty of conducting experiments at high temperatures. *Methanococcoides burtonii* is a psychrophilic archaeon with an optimal growth temperature of 21°C [2]. The genome of *M. burtonii* encodes two sHSPs (MbHsp19.8 and MbHsp17.3). In this study, we aimed to elucidate the temperature-dependent oligomeric dissociation mechanism of sHSP by performing structural and functional analyses of sHSP oligomers under heat stress using MbHsp17.3.

EXPERIMENTS: The synthetic DNA of MbHsp17.3 was cloned into pCold IV vector. Using the plasmid, MbHsp17.3 was expressed in *E. coli* BL21(DE3), then purified using anion exchange chromatography, hydrophobic chromatography, and gel filtration chromatography. Structural analysis was conducted using analytical ultracentrifugation (AUC) and small-angle X-ray scattering (SAXS). To assess the temperature and concentration dependence of oligomer dissociation, analytical ultracentrifugation measurements were performed at various temperatures and concentrations. Chaperone functional was analyzed by the aggregation inhibition effect on citrate synthase (CS).

RESULTS: The oligomers of MbHsp17.3 were confirmed to dissociate temperature- and concentration-dependently from the results of AUC (Fig 1). interestingly, at 40°C, the oligomers nearly completely dissociated, with various smaller structures detected, albeit with a decreased amount simultaneously detected. This suggests the formation of aggregates not detectable by AUC at high temperatures. At 4°C, there were oligomeric structures of 20 subunits or more, but measurements at 25°C showed the main peak at 16 subunits, which was confirmed to be a structure close to 16 subunits by SAXS analysis. MbHsp17.3 was suggested to form similar 24 subunit oligomers to other archaeal sHsps at low temperatures and exhibit activity at 16 subunits. Weak aggregation inhibition activity was confirmed by CS aggregation suppression assay.

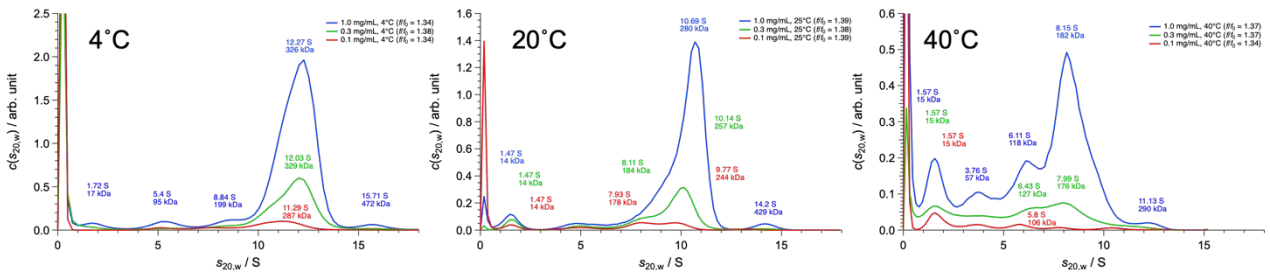

Fig. 1. AUC results of MbHsp17.3 at 4 °C, 25 °C, and 40 °C

REFERENCES:

[1] N. Kurokawa *et al.*, Int J Mol Sci., **22** (2021) 10797.
[2] P. D. Franzmann *et al.*, Syst. Appl. Microbiol., **15** (1992) 573–581 115-120.

CO6-8

Visualization of intrinsically disordered structure of F_1-ATPase ε subunit through integration of AUC-SAXS measurement and MD simulation

T. Oroguchi[1], K. Morishima[2], R. Inoue [2], M. Sugiyama[2], Y. Yamada[3]

[1] *Department of Physics, Faculty of Science and Technology, Keio University*
[2] *Institute for Integrated Radiation and Nuclear Science, Kyoto University*
[3] *Department of Life Science, College of Science, Rikkyo University*

INTRODUCTION: The ε subunit of F_oF_1-ATPase synthase plays as an intrinsic regulator of ATPase activity of F_1-ATPase depending on ATP concentration. The C domain of this subunit is an intrinsically disordered region, and the specific binding to ATP induces the structural formation of this domain and switches the inhibitory state off [1,2]. Furthermore, it has been recently reported that the disordered structure of the ε subunit is also involved in regulating the rotational coupling between F_o and F_1-ATPase [3]. Therefore, to elucidate the regulatory mechanism by the ε subunit, it is necessary to visualize its disordered structure. However, such visualization is difficult for the existing structural analyses methods such as X-ray crystal structure analyses, cryo-electron microscopy, etc. In this study, we challenge to visualize the disordered structure of the ε subunit through the technique integrating SAXS experiments and MD simulation [4]. Due to its tendency to aggregate, the ε subunit was measured using AUC-SAXS [5], which allows to confirm oligomeric states during measurement. **********

EXPERIMENTS: We condensed the purified isolated ε subunit to a concentration of 4 mg/ml, where SAXS intensity could adequately obtained, and conducted AUC-SAXS measurements. The measurements were conducted for both the ATP-unbound and the ATP-bound states. The ionic strength of the measurement buffer was adjusted to 150 mM to minimize aggregation.
****

RESULTS: Through the present measurements, we were able to observe the structural change of the ε subunit due to ATP binding (Fig. 1A), consistent with the previous biochemical data [1,2]. The SAXS data revealed that the adopted condensation protocol and measurement conditions allowed us to obtain the non-aggregated ε subunit. However, the AUC also showed that at the used concentration, the ε subunit exists in a monomer-dimer equilibrium for both ATP-unbound and ATP-bound states (Fig. 1B). We additionally conducted the AUC measurements for the lower concentration, and the results revealed that the equilibrium shifted to the monomeric state. From all these results, we established the sample preparation protocol and measurement condition, which allow us to obtain the data for the isolated ε subunit at the next measurement.
****

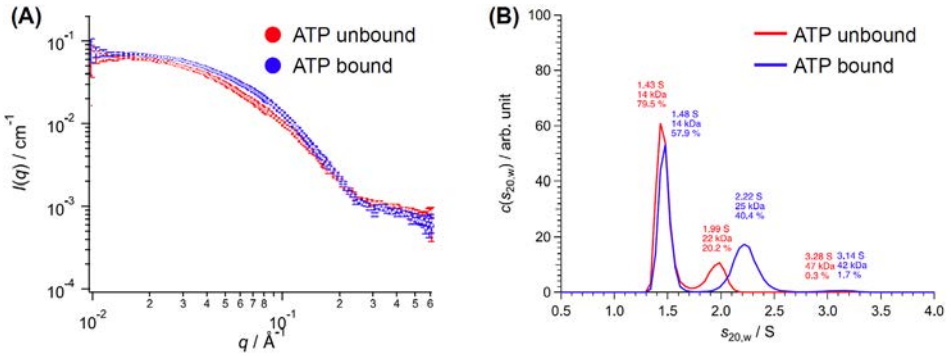

Fig. 1 (A) SAXS data, (B) AUC data of the ε subunit.

REFERENCES:

[1] Y. Kato-Yamada & M. Yoshida, J. Biol. Chem., **278** (2003) 36013-36016.
[2] S. Kato, M. Yoshida & Y. Kato-Yamada, J. Biol. Chem., **282** (2007) 37618-37623.
[3] F. Kadoya, S. Kato, K. Watanabe & Y. Kato-Yamada, Biochem. J., **437** (2011) 135-140.
[4] T. Oroguchi *et al.*, Biophys. J., **96** (2009) 2808-2822 .
[5] K. Morishima *et al.*, Comm. Biol., **3** (2020) 294.

CO6-9

Change of Microglia/ Macrophage after immuno- and/or radiation therapy

N. Kondo[1], Y. Shimizu[2], and Y. Sakurai[1]

[1] *Particle Radiation Oncology Research Center, Institute for Integrated Radiation and Nuclear Science, Kyoto University (KURNS)*

[2]*Dept. of Diagnostic Imaging and Nuclear Medicine, Graduate School of Medicine, Kyoto University.*

INTRODUCTION: Radiotherapy such as X-rays and γ-rays is used as a standard treatment as a safe and effective cancer treatment. After radiation therapy, vascular permeability increases in the irradiated tissue, and infiltrating immune cells increase then causing inflammation. There are many unknown points, such as the interaction between infiltrated immune cells and residual tumors in the microenvironment, the effects of immune cells on organs and tumors outside the irradiated area. In addition, immune checkpoint inhibitors have come into use, and interactions mediated by immune cells have been emphasized. Also, abscopal effect is boosted with immunotherapy [1]. In this study, we investigated how immune cells (macrophages, regulatory T cells, cytotoxic T cells, etc.) infiltrate and interact with irradiated tissues and organs throughout the body (outside the field of irradiation), including the brain, after irradiation. We will also investigate the changes that occur when immune checkpoint inhibitors are used in combination with radiation therapy.

EXPERIMENTS:

Cells:

We used Lewis Lung Cell Carcinoma cell line (LLC). They were cultured in RPMI 1640 medium with 10% heat-inactivated fetal bovine serum in 5 % CO_2 incubator.

Innoculation of tumor and drug treatment to animals

We used C57BL/6 mice. $5E^5$ LLC cells were inoculated subcutaneously in a thigh of the mice. We created four groups (non-treatment, immunotherapy alone, radiation therapy alone, and immunotherapy and radiation therapy combined) and each group contained 9 animals. After the inoculation, we administrated anti-mouse PD-1 antibody on the day 6 and 12 (250 μg/body).

Irradiation:

We used the Cobalt 60 gamma-ray irradiation device in KURNS. On the day 13, we irradiated the tumor on the thigh of mice at the dose of 20 Gy shielding the body and head with lead.

Measurement of tumor size and sampling of tumors and brains

After the irradiation, we measured the major and minor axes of the tumors until mice were sacrificed. We sacrificed three mice in each group on 2, 7, 14 days after irradiation. The brain and tumor were removed and fixed in 10 % buffered formalin for pathological samples.

Immunohistochemistry:

We prepared paraffin sections, and stained microglia or macrophages using a monoclonal Iba-1 antibody for 1st antibody. DAB staining was used for second antibody. We analyzed the numbers of Iba-1 positive cells in the hippocampus and cortex of the brain or in the tumor.

RESULTS:

Tumor size: Only in the combination group, tumor size was significantly reduced compared with the control at 14 days after irradiation.

Pathology: The number of microglia in hippocampus tended to increase in immunotherapy alone group at 2 days after irradiation. We still continue counting.

REFERENCES:

[1] Ngwa W. *et.al.,* Nat Rev Cancer.; **18(5)** (2018) 313-322. (doi)10.1038/nrc.2018.6.

CO6-10

Growth of transthyretin amyloid protofibrils monitored by AUC and SAXS

N. Yamamoto[1], K. Morishima[2], R. Inoue[2], E. Chatani[3], M. Sugiyama[2]

[1]*Schoole of Medicine, Jichi Medical University*
[2]*Institute for Integrated Radiation and Nuclear Science, Kyoto University*
[3]*Graduate School of Science, Kobe University*

INTRODUCTION: Transthyretin (TTR) is a blood protein required for transporting thyroxine and retinol to liver. TTR is composed of 127 amino-acid residues forming a homo tetramer in a physiological condition. TTR is known to form amyloid fibrils which are abnormal protein aggregates composed of β-sheet stacked structure along with the fibril axis. TTR amyloid fibrils accumulate in various kinds of organs such as heart. As a result, their functions are lost, which finally leads death of patients. Therefore, understanding the mechanism of the amyloid fibril formation of TTR is required to find ways for preventing the accumulation of the fibrils. Recently, we found that protofibrils appear prior to the emergence of the TTR amyloid fibrils in vitro, which finally convert to the amyloid fibril (unpublished data). In this study, we tracked the growth of the protofibrils using small-angle X-ray scattering (SAXS) and analytical ultra centrifuge (AUC).

EXPERIMENTS: Wild type TTR at the concentration of 100 μM in 10 mM HCl was incubated at 75 °C. AUC was performed at a few time points at 25 °C using XL-I (Beckman Coulter, Indiana). SAXS profiles were obtained using a SAXS equipment, NANOPIX (Rigaku, Japan) at the same time points as AUC at 25 °C.

RESULTS: Figure 1 shows the result of AUC. At 1 h, only one peak is observed at around 9.4 S. However, at 16 h another peak appeared around 28 S. This peak shifted larger as a function of time, which finally became around 50 S at 48 h. These results are consistent with our previous observation that the protofibrils become longer as a function of time.

The SAXS profiles are shown in Figure 2. Overall intensities decrease as a function of time. Whereas the intensity starts to get flat as q decreases at 1 h at the low-q region, the intensity continues to increase as q decreases at 24 h or 48 h. These results indicate that the decrease in the overall intensities as a function of time is due to the low-q shift of the SAXS profiles due to the formation of larger components. The interpretation is consistent with the results observed in AUC.

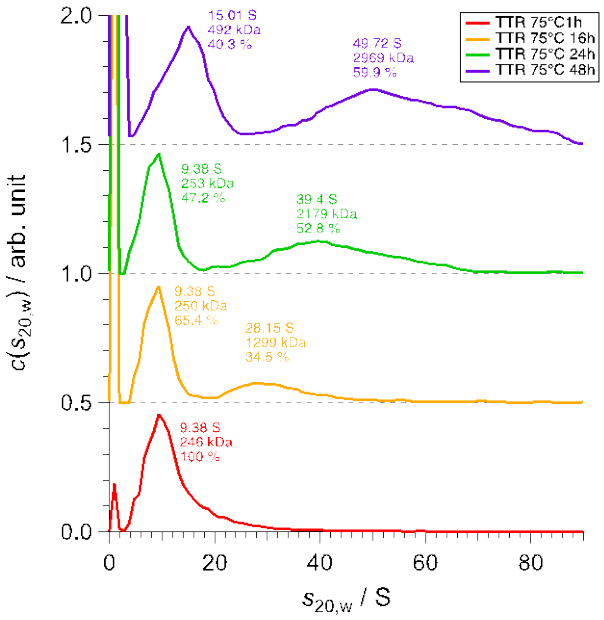

Figure 1 and 2. The AUC profiles (Figure 1; left) and SAXS profiles (Figure 2; bottom), respectively.

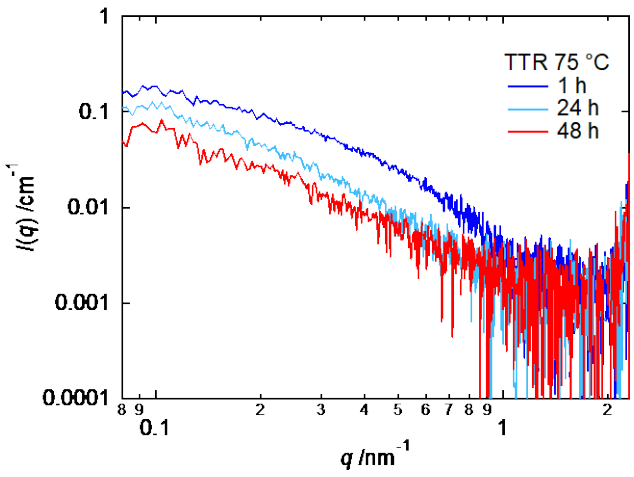

CO6-11

Evaluation of radiation resistance of lens constituent proteins involved in age-related cataract

T. Takata and K. Lampi[1]

Institute for Integrated Radiation and Nuclear Science, Kyoto University
[1] Oregon Health & Science University

INTRODUCTION: The transparency of the lens is maintained by the stable long-lived protein interactions, comprising three kinds of crystallin families. Those proteins are very stable, but are decreased their stability with age. A kind of intrinsic damages of lens tissues, such as heat damage, or extrinsic damages such as UV damage are increased with life time. Several researches suggested the amount of heat/UV damage on lens crystallins could be well described by the amount of modifications of amino acid residues [1]. When the crystallin species or partially model peptides are subjected to high intensity oxidative stress, site-specific oxidative modifications of amino acids accumulated [2]. This is analogous to the disease manifestations of sunlight-induced age-related cataracts. Due to the technical troubles, we lost the model peptides of lens crystallin after γ-rays irradiation before LC-MS analysis. Therefore, in order to observe irradiation effect for lens components, we performed γ-ray irradiation (50–5000 Gy) to recombinantly human βB2-crystallin oxidation mimic proteins (βB2 mimics) again, and evaluated solubilities for each protein.

EXPERIMENTS: Each of five tryptophan residue (Trp) in βB2-crystallin was replaced by phenylalanine residue (Phe) respectively by site-directed mutagenesis to make βB2 mimics (W59F, W82F, W85F, W151F and W196F). Each sample were prepared to 1 mg/mL in 50 mM phosphate buffer (pH 7.0) in 1.5 mL polypropylene tubes, and were irradiated with 0 (control), 50, 500, and 5000 Gy of γ-rays using a $_{60}$Co γ-ray source installed at the Institute for Integrated Radiation and Nuclear Science, Kyoto University. After γ-ray irradiation, each tube was centrifuged at 15,000 x g for 10 minutes at 4°C, and the protein concentration in the soluble fraction was measured using Bio-Rad's protein assay kit. The % of βB2 mimic is obtained from the formula on the right.

$$\text{[Protein] in soluble fraction [\%]} = \frac{\text{[Protein] after irradiation}}{\text{[Protein] at 0 Gy}} \times 100$$

RESULTS: A dose-dependent decreasing of the amount of βB2 mimics was observed in the γ-ray -irradiated βB2 mimics compared to the non-irradiated recombinantly human βB2-crystallin (Fig. 1). All samples showed a decreasing trend in the amount of crystallin in the soluble fraction as a function of irradiation dose. A slight decreasing the amount of soluble fraction after γ-irradiation was observed, however no significant difference could be obtained. Since some proteins were adhered to the inner wall of each tube on high dose experiments as white layer, we considered that those may cause huge error at each of dose and uncertain similarities at high dose. The irradiation may induce abnormal sticky protein state in solution.

Fig. 1. Aggregation tendency of βB2 mimics due to reduced oxidative stress tolerance

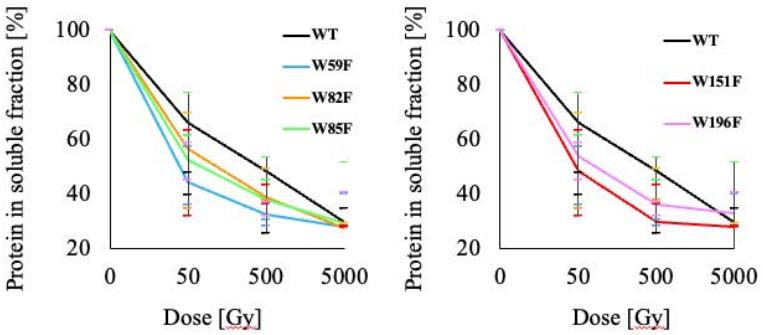

REFERENCES:

[1] B. Searle *et al.*, J Proteome Res., **4** (2005) 546-554.
[2] I. Kim *et al.*, Biochem Biophys Res Commun., **466** (2015) 622–628.

CO6-12

Solution strcuture of protein under high pressure as studied by small-angle scattering and molecular dynamics simulation

R. Inoue, N. Aizawa, M. Shimizu, K. Morishima and M. Sugiyama

Institute for Integrated Radiation and Nuclear Science, Kyoto University

INTRODUCTION: The free-energy landscape of protein is strongly perturbated by the application of high pressure, promoting the denaturation of protein. In fact, pressure denaturation has been experimentally reported for proteins with small molecular weight. However, it is also reported that special proteins from high-pressure environments (e.g., the deep sea) maintain their folded conformation even under high pressure and express their biological functions. Therefore, analysis of solution structure and dynamics of these proteins under high pressure is strongly expected to elucidate the structural stability mechanism of proteins under high pressure. Here, we especially focused on GSJ, an α-glucosidase derived from a deep-sea microorganism (Geobacillus sp. HTA-462). As shown in Fig.1, the crystal structure of GSJ has already been reported, however the solution structure of GSJ under high pressure has not yet been clarified. Therefore, we determined to elucidate the solution structure of GSJ under high pressure through the combination of small-angle scattering experiments and all-atom molecular dynamics (MD) simulations.

Fig. 1 Schematic view of structure of GSJ.

EXPERIMENTS: High pressure small-angle neutron scattering measurement was performed with SANS-U of the Institute for Solid State Physics, University of Tokyo, installed at JRR-3 (Tokai, Japan). Utilizing high pressure cell, solution structures of GSJ solution at 0.1 MPa and 100 MPa were studied. All-atom MD simulation under high pressure was performed by inserting water molecules inside the protein.

RESULTS: Figure 2 shows the scattering profiles of GSJ solution at 0.1 MPa and 100 MPa. It is clearly seen that the SANS profile at high pressure is significantly different from that at ambient pressure. To exhibit the structural perturbation by high pressure, we analyzed the radius of gyration (R_g) at two pressure conditions. At ambient pressure, it was calculated that R_g value was 25.3±2.8 Å. On the other hand, R_g value at 100 MPa was increased to 53.6±13.1 Å, meaning an experimental detection of denaturation at high pressure. In the case of living organism at deep sea, the concentration of osmolyte such as trimethyl amino-oxide is high compared to those at ambient pressure. Hence, the absence of osmolyte in GSJ solution is mainly concerned for the observation of denaturation at 100 MPa from the present SANS measurements. Figure 3 shows time dependence of R_g value calculated from all-atom MD simulation under high pressure. It was revealed that R_g value from the MD simulation reached to the R_g value from SANS measurements, supporting the possibility of reproduction of high pressure induced denaturation of protein from present MD simulation. Further calculation is still on progress to validate the present results from MD simulation.

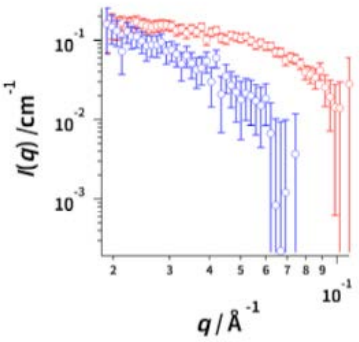

Fig. 2 SANS profiles of GSJ solution at 0.1 MPa (red circle) and 100 MPa (blue circle).

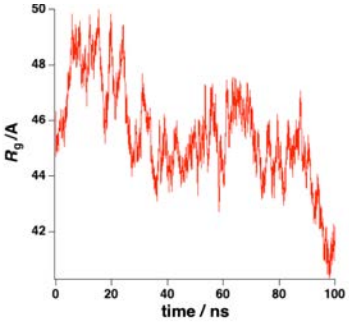

Fig. 3 Time course of from all-atom MD simulation.

CO6-13

Solution structure of proteasome α7 double ring

K. Kato[1,2,3], M. Yagi-Utsumi[1,2,3], S. Yanaka[1,2,3], H. Yagi[1,2], T. Satoh[1], Y. Yunoki[4], K. Morishima[4], R. Inoue[4] and M. Sugiyama[4]

[1]*Graduate School of Pharmaceutical Sciences, Nagoya City University*
[2]*Exploratory Research Center on Life and Living Systems (ExCELLS), National Institutes of Natural Sciences*
[3]*Institute for Molecular Science, National Institutes of Natural Sciences*
[4]*Institute for Integrated Radiation and Nuclear Science, Kyoto University*

INTRODUCTION:

Proteasomes are large protein complexes involved in cellular proteolysis and are widely distributed across the three domains of life. The 20S proteasome is the core complex of the eukaryotic proteasome composed of layered α and β heptameric rings. The α and β heptameric rings are composed of seven different homologous subunits each, α1–α7 and β1–β7. Interestingly, the α7 subunit forms a homotetradecamer consisting of two layers of α7 heptameric rings (α7 double ring) [1,2]. The structure of the α7 double ring in solution has not been fully revealed. In this study, we investigated its solution structure with small-angle X-ray scattering (SAXS).

EXPERIMENTS:

The human proteasome α7 subunit was expressed and purified as described previously [1, 2]. The sample was dissolved in a buffer containing 20 mM Tris-HCl (pH 8.0) and 150 mM NaCl. SAXS measurement was carried out with NANOPIX (Rigaku) installed in KURNS at 25 ºC. The *q*-range (magnitude of the scattering vector) covered was from 0.010 Å-1 to 0.70 Å-1, using two sample-to-detector distances (SDD) of 1333 and 295 mm. To remove the effect of non-specific aggregates on the SAXS profile, we applied the integrated reduction method utilizing analytical ultracentrifugation (AUC) and SAXS, namely AUC-SAXS [3,4]. AUC measurement was conducted with ProteomeLab XL-I (Beckman Coulter) at the rotation speed of 60,000 rpm at 25 ºC.

RESULTS:

Figure 1 displays the SAXS profile of the proteasome α7 double ring. The candidate structure obtained from Cryo-EM (model 1) did not completely match the experimental SAXS profile. Thus, we performed the normal mode analysis (NMA) using model 1 as the initial structure to search appropriate structural model in solution. As a result, we found that a structure in which the α7 ring (model 2) was significantly deformed compared to model 1 reproduced the SAXS profile.

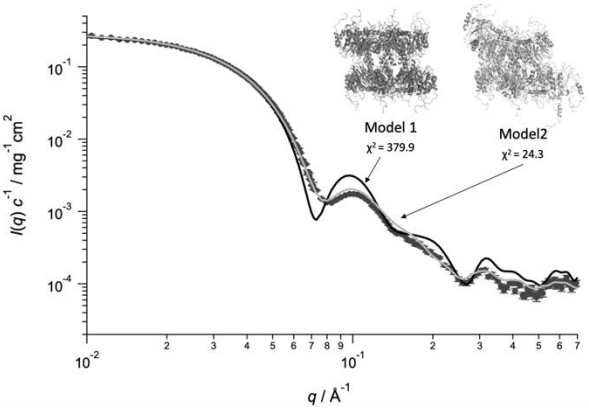

Fig. 1. Black circles represent SAXS profile of the proteasome α7 double ring. Solid black and gray lines show the scattering curves calculated from model 1 and 2, respectively.

REFERENCES:

[1] M. Sugiyama *et al.*, Biophys. J., **101** (2011) 2037-2042.
[2] C. Song *et al*., Int. J. Mol. Sci., **22** (2021) 4519.
[3] K. Morishima *et al.,* Commun. Biol., **3** (2020) 294.
[4] K. Morishima *et al.,* J. Appl. Crystallogr., **56** (2023) 624.

CO6-14

SAXS study on the interaction manner between the α-crystallin domain of αB-crystallin and insulin B-chain protofibrils

Y. Kokuo, K. Yuzu, N. Yamamoto[1], K. Morishima[2], A. Okuda[2], R. Inoue[2], M. Sugiyama[2], J. Hayashi[3], J. A. Carver[3], E. Chatani

Graduate School of Science, Kobe University
1Graduate School of Medicine, Jichi Medical University
2Institute for Integrated Radiation and Nuclear Science, Kyoto University
3Research School of Chemistry, The Australian National University

INTRODUCTION: Amyloid fibrils are protein aggregates involved in amyloidoses and neurodegenerative diseases. A cellular strategy for preventing the formation of amyloid fibrils is the expression of small heat shock proteins (sHsps), of which αB-crystallin (αB-C) is a representative member in mammals. Our previous measurements have shown that the α-crystallin domain (ACD) of αB-C inhibits the growth of insulin B-chain protofibrils strongly [1]. In this study, to gain insights into the binding manner of the ACD with B-chain protofibrils, a small-angle X-ray scattering (SAXS) measurement was performed in combination with analytical ultracentrifugation (AUC).

EXPERIMENTS: Insulin B-chain was dissolved at a final concentration of 400 μM in 50 mM Tris-HCl buffer (pH8.7) and incubated at 25 °C to form protofibrils. After the ACD was mixed with the protofibrils in a molar ratio of B-chain:ACD = 1:0.1, the samples were then subjected to SAXS measurements to investigate changes in size and shape of protofibrils in the presence of the ACD. A SAXS profile was collected at 25 °C and 30-minute exposure with a NANOPIX equipped with a HyPix-6000 (Rigaku Corpo-ration, Japan). A Cu K-α line (MicroMAX-007HFMR) was used as a beam source, which was further focused and collimated with a confocal multilayer mirror (OptiSAXS). The camera length was set to 1.33 nm.

RESULTS: As shown in Fig. 1A, the slope of the log-log plot was close to −1, suggesting that protofibrils keep a rod-like morphology even after the ACD binding. When a cross-section plot was constructed, the slope of this plot did not show any significant change as shown in Fig. 1B. This is contrastive to the result of full-length αB-C, in which the complex become thicker after the binding to protofibrils [2]. Although the length was difficult to be estimated from the SAXS profile because of limited *q* range, it has been suggested that the αB-C ACD tends to bind to the protofibril edges rather than the side, preventing further protofibril growth. It is likely that the remaining domains, i.e., the N- and C-terminal domains, mediate lateral binding to the protofibril, and which may not be important for inhibition of protofibril growth.

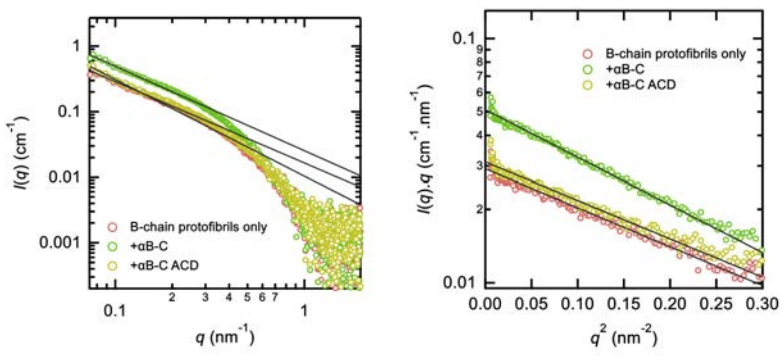

Fig. 1. (A) SAXS profiles and (B) their cross-section plots of the insulin B-chain-αB-C ACD complex. The profiles of B-chain alone and B-chain-αB-C complex are also shown for references. The fraction of unreacted αB-C ACD or αB-C estimated from the AUC analysis was subtracted from the SAXS profile to obtain the profiles of the complex selectively.

REFERENCES:

[1] Y. Kokuo, Master Thesis, Kobe Univ. (2023).
[2] Y. Kokuo, KURNS Progress Report 2022, (2023) CO6-9.

CO6-15

Development of Boron Cluster-Loaded Nanoparticles for BNCT

A.B. Fithroni[1], M. Ishimoto[2], K. Watanabe, H[1]. Inoue, S[1]. Zhou, T.F.N. Hakim[1], M. Suzuki[3], T. Ohtsuki[1], and E. Matsuura[1]

[1]*Department of Interdisciplinary Science and Engineering in Health Systems, Okayama University*
[2]*J-BEAM, Inc.*
[3]*Institute for Integrated Radiation and Nuclear Science, Kyoto University*

INTRODUCTION: Boron neutron capture therapy (BNCT) is a non-invasive nuclear therapeutic modality that induces apoptosis in cancer cells, without any harmful effects in neighboring normal cells. To overcome the issues of limited application in clinically approved boron compounds, such as BPA and BSH, we developed self-forming nanoparticles consisting biodegradable polymer, namely, "Lactosome micelles" with a hydrophobic boron cluster [1]. In the previous study, we were able to develop a stable Lactosome micelles highly loaded with a hydrophobic boron cluster that may be applicable for BNCT [2]. Currently, we evaluated the efficacy of *in vitro* and *in vivo* neutron irradiation to the AsPC-1 cells (human pancreatic cancer cells) or those derived tumors in xeno-grafts which were treated with a boron cluster-loaded Lactosome micelles.

EXPERIMENTS: For *in vitro* study, we irradiated AsPC-1 cells were subjected with reactor power of 1 MW for 40 min after incubation with a boron cluster-loaded Lactosome micelles for 2 h. After the neutron irradiation, colony formation assay was performed by culturing in 12-well plates and incubated under 5% CO_2 at 37 °C for 14 days. For *in vivo* study, the AsPC-1 cells-bearing ice were intravenously (*i.v.*) injected with a boron-cluster loaded Lactosome micelles, and then, the neutron irradiation was performed with nuclear power of 5 MW for 40 min. Data were represented as mean ± S.E.M. Significant differences were represented by $^{**}p < 0.01$ and $^{*}p < 0.05$.

RESULTS: In *in vitro* irradiation study, the results obviously indicated that boron cluster-loaded Lactosome micelles showed significant inhibitory effect in the colony formation of the AsPC-1 cells (Table 1). *In vivo* irradiation study also showed that a group *i.v.* injected with boron cluster-loaded Lactosome micelles by irradiating with neutron significantly suppressed the tumor growth on day 24 after irradiation, as compared to cold control and hot control (Table 2). Overall, *in vitro* and *in vivo* neutron irradiation study showed that our novel development of boron cluster-loaded Lactosome micelles are promising candidates (drug) for BNCT.

Table 1. *In vitro* inhibitory effect by neutron irradiation on AsPC-1 cells' growth under the treatment with boron cluster-loaded Lactosome micelles.

Group	Colony formation rate	
	0 min	40 min
Control (DPBS)	1	0.73 ± 0.41
Lactosome micelles	1	0.53 ± 0.16
-loaded with boron cluster A	1	0.03 ± 0.01**
-loaded with boron cluster B	1	0.05 ± 0.00**

Table 2. *In vivo* inhibitory effect by neutron irradiation on AsPC-1 cell-derived tumors' growth under the treatment with boron cluster-loaded Lactosome micelles.

Group	Percent of tumor growth on days 24
Control (cold)	315.7 ± 89.4
Control (hot)	195.0 ± 39.3
Lactosome micelles	
- loaded with boron cluster A	62.9 ± 17.6**
- loaded with boron cluster B	12.0 ± 19.7**

RFERENCES:

[1] E. Hara *et al.*, Biochim Biophys Acta., **1830** (2013) 4046–4052.
[2] Fithroni, A.B. *et al.,* Cells, **11** (2022), 3307.

CO6-16

Asp racemization/isomerization in shedding products of cell adhesion molecule 1 is potentially involved in the neurodegeneration induced by elevated pressure

A. Yoneshige[1], A. Ito[1] and T. Takata[2]

[1]*Department of Pathology, Kindai University*
[2]*Institute for Integrated Radiation and Nuclear Science, Kyoto University*

INTRODUCTION: The elevation of internal pressure is often involved in neurodegeneration; intraocular and intraventricular pressure elevations over 20–30 cmH2O cause glaucoma and hydrocephalus, respectively. Previously, to investigate the mechanisms by which elevation of intraluminal pressure causes cell or tissue de-generation, we devised a novel two-chamber culture system that enabled us to subject cultured cells to low levels of water pressure (2-50 cmH2O pressure load) [1,2]. We found that mouse primary neurons degenerated when the water pressure was above 30 cmH2O, and that ectodomain shedding of synaptic cell adhesion molecule 1 (CADM1) increased in a water pressure-dependent manner [1]. We also discovered that the increase of intracellular product of CADM1 shedding (C-terminal fragment, CADM1-CTF) resulted in decreased neurite density with punctate localization of CADM1 suggesting its aggregation in neurites [1]. CADM1-CTF is rich in Asp residues neighbored by Ala residues, and the conversion of these amino acids to poly-Gly diminished its aggregation state. Since the racemization and isomerization of Asp residues contributes to aggregation of various proteins and it likely occurred when the neighboring residues are small [3,4], these in-sights led us to hypothesize an involvement of Asp racemization/isomerization in the neurodegeneration induced by internal pressure elevation.
EXPERIMENTS: (1) Synthetic peptide of internal sequence of CADM1-CTF (GADDAADAD-TAIINAEGGQNNSEEK) was incubated at 50℃ for 0-15 days and applied to LC-MS to identify Asp isomer-containing peptides. (2) Mouse neuroblastoma cell line Neuro-2a cells with exogenously expressed CADM1-CTF were cultured un-der 50 cmH2O and were prepared for LC-MS analysis. (3) To mimic oxidative stress induced by internal pressure elevation, Neuro-2a cells expressing CADM1-CTF were treated with hydrogen peroxide and the cells were subjected to the isolation of CADM1-CTF by immuno-precipitation (IP). The amounts and purity of CADM1-CTF-IP were quantified using immunoblotting and silver staining.
RESULTS: (1) In LC-MS analysis of CADM1-CTF synthetic pep-tide, multiple peaks were detected after 1 day at pH 6.0 or pH 7.0 indicating that Asp racemization/isomerization could occurred under neutral pH. (2) CADM1-CTF proteins in Neuro-2a cells were solubilized with water, Triton X-100 containing buffer, or SDS containing buffer after 3 days culture under 50 cmH2O, and CADM1 immunoblot was carried out. CADM1-CTF protein yields (CADM1-CTF / total proteins) were in the order Triton X-100 > SDS > water, however, the peptide peak was not identified using with LC-MS. (3) Previously, we found that CADM1 shedding was increased by oxidative stress as a cause of pulmonary emphysema in cigarette smoke exposure [5]. We furthermore showed that Lipocalin-2, an iron binding protein was upregulated in the retinae under 50 cmH2O pressure [6]. Since iron dysregulation induces oxidative stress, we decided to explore the linkage between oxidative stress and Asp racemization/isomerization of CADM1-CTF. We successfully obtained a huge amount of partial purified CADM1-CTF from large-scale Neuro-2a cell culture, coupled with IP purification. Future experiments are planned for identification of Asp isomer by LC-MS.
REFERENCES: [1] A. Yoneshige *et al.,* Mol. Neurobiol., **54** (2017) 6378-6390. [2] M. Hagiyama *et al.,* Front. Physiol., **8** (2017) 997. [3] N. Fujii *et al.,* J. Biochem., **116** (1994) 663-669. [4] T. Takata *et al.,* Protein Sci., **29** (2020) 955-965. [5] A. Ri *et al.,* Front. Cell Dev. Biol., **6** (2018) 52. [6] A. Yoneshige *et al.,* Front. Cell Dev. Biol., **9** (2021) 664327.

CO6-17

The regulation of the cyanobacterial circadian rhythm by KaiC hexamers capable of assuming diverse phosphorylation states

Y. Yunoki[1], K. Morishima[2], N. Sato[2], R. Inoue[2], A. Okuda[2], R. Urade[2], M. Sugiyama[2]
[1]*Center for iPS Cell Research and Application, Kyoto University*
[2]*Institute for Integrated Radiation and Nuclear Science, Kyoto University*

INTRODUCTION: The circadian rhythm is controlled by clock proteins. In cyanobacteria, the clock operates through interactions among KaiA, KaiB, and KaiC, resulting in a cyclic oscillation of KaiC phosphorylation facilitated by ATP. KaiC forms a homohexamer and exhibits ATPase activity during autophosphorylation and dephosphorylation processes. Despite the potential for up to 700 phosphorylation states within the KaiC hexamer due to the presence of two phosphorylation sites per subunit, previous studies have only showed the average phosphorylation state of the KaiC hexamer. To address the oscillation mechanism, we have developed native mass spectrometry to simultaneously analyze the phosphorylation states within the KaiC hexamer and the interactions between Kai proteins, such as the KaiB-KaiC interaction.
****

EXPERIMENTS: nMS measurements were conducted using a microTOF II ESI mass spectrometer (Bruker) at room temperature, employing the microTOF II software. KaiB and KaiC proteins derived from thermophilic cyanobacteria, T. elongatus BP-1, were produced in Escherichia coli and purified through anion-exchange chromatography and size-exclusion chromatography. To manipulate the phosphorylation state within the KaiC hexamer, two KaiC mutants, $KaiC_{AA}$ and $KaiC_{DD}$ (where Ser431 and Thr432 were substituted with aspartate and alanine residues, respectively), were employed to mimic the dephosphorylated and phosphorylated states of KaiC, respectively. To create a heterogeneous phosphorylation state group within the KaiC hexamers, prior to ATP addition, we combined unlabeled $KaiC_{AA}$ mutant and ^{13}C-labeled $KaiC_{DD}$ subunit. This strategy enabled the generation of seven different types of KaiC hexamers with distinct phosphorylation states.
****

RESULTS: We successfully generated a heterogeneous phosphorylation state group within the KaiC hexamer (Fig. 1). Then, we decided to elucidate the KaiB-KaiC interaction.
Our findings, shown in Fig. 1, demonstrate that the KaiB-KaiC interaction is determined by the proportion of KaiCDD subunits within the KaiC hexamer. The KaiB-KaiC complex facilitates the dephosphorylation of KaiC. Based on our observations, it is hypothesized that KaiC promotes its own dephosphorylation by binding to KaiB when it becomes hyperphosphorylated.
We propose that KaiC modulates the KaiB-KaiC interaction through alterations in the phosphorylation state of the KaiC hexamer. We anticipate that these findings will enhance our understanding of the oscillation mechanism involving the dissociation and assembly of Kai proteins.

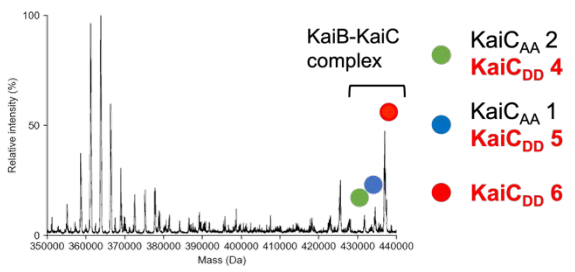

Fig. 1. KaiB-KaiC interaction is regulated by the KaiC hexamer phosphorylation state.

The native mass spectra depict a heterogeneous phosphorylation state within the KaiC hexamer in the presence of KaiB. The circles represent the KaiB-KaiC complex, with green, black, and red circles indicating KaiC hexamers comprised of different ratios of $KaiC_{AA}$ and $KaiC_{DD}$ subunits, specifically 2:4, 1:5, and 0:6, respectively.

****

CO6-18

Analysis of flexible structure of flexible multi-domain protein

T. Oda, R. Inoue[1], K. Morishima[1], A. Okuda[1], M. Sugiyama[1]

J-PARC Center, Japan Atomic Energy Agency.
[1]Institute for Integrated Radiation and Nuclear Science, Kyoto University.

INTRODUCTION: Proteins that are composed of multiple domains and intrinsically disordered regions (IDRs) are flexible and perform various biological functions. Their flexible nature makes it difficult to analyze their structures by crystallography or cryo-electron microscopy. In this study, we focused on a DNA repair protein Hef from hyperthermophilic archaeon as a flexible muti-domain protein and attempt to determine the flexible structure as an ensemble using SAXS and SANS. Hef consists of an N-terminal helicase domain, a C-terminal nuclease domain, and an IDR connecting the two domains [1,2]. From SAXS analysis using only the IDR, we found that IDR becomes more compact at high temperatures (323K ~ 363K) than at room temperature. Considering the physiological temperature of hyperthermophilic archaeon, we speculate that this compaction is related to the function of Hef. Therefore, we attempted to analyze structure of full-length Hef at high temperature (353K). Since the entire molecule contributes to scattering in SAXS, it is difficult to determine the ensemble structure of a multi-domain protein based solely on the SAXS profile. Therefore, to obtain another experimental constraint, we prepared a full-length Hef protein with 75% deuteration in only the helicase or the nuclease domain (segmentally deuterated samples, Fig.1(a)) and measured SANS. Note, in 100% D_2O, the 75% deuterated domain is matched out, and only scattering of the non-deuterated region can be observed. Therefore, it is expected that the ensemble structure can be determined correctly by combining it with the SAXS profile.

EXPERIMENTS: The segmentally deuterated samples were prepared by ligation the 75% deuterated domain and the non-deuterated region using a protein ligation enzyme. Since Hef tends to aggregate, we performed size exclusion chromatography to remove aggregates and performed SANS measurements using a dilute sample (0.6 mg/ml). The SANS measurements were performed with SANS-U installed at JRR-3. To check for the presence of aggregates, the sample solution after SANS measurement were analyzed by analytical ultracentrifugation (AUC).

RESULTS: The SANS profiles of the segmentally deuterated samples at 353K are shown in Fig. 1(b). The SANS profiles did not show any sharp rise at the low angle. Thus, at first glance it appears that there are no aggregates in the samples. However, the AUC analysis of the sample after SANS measurement, indicated the presence of aggregates and degradant (Fig. 1(c)). In this experiment, we performed long exposure time (totally 16 and 24 hours for each sample) to obtain data with sufficient statistical accuracy from extremely dilute samples. Therefore, it is possible that aggregates and degradant were generated during long-time experiments. It will be necessary to consider experimental conditions that prevent aggregation and degradation.

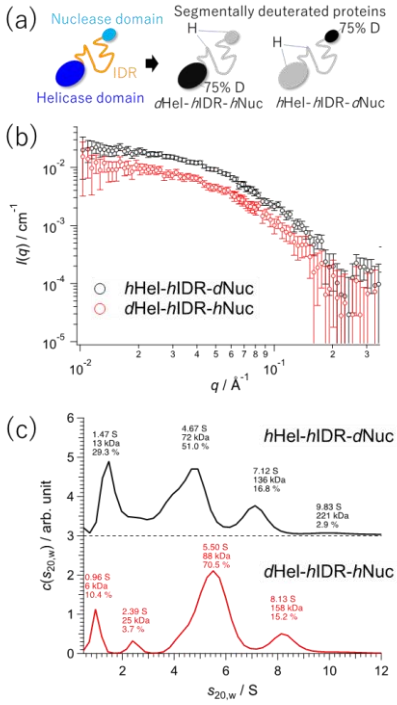

Fig 1. Schematic view of segmentally deuterated proteins (a) and its profiles of SANS (b) and AUC (c).

REFERENCES: [1] R. Fujikane *et al.,* Genes Genet. Syst., 85 (2010) 243.
[2] S. Ishino *et al.,* J. Biol. Chem., 289 (2014) 21627.

CO6-19

Character of DNA damage induced by nuclear plant neutron beams

H. Terato, T. Hanafusa[1], M. Isobe, Y. Sakurai[2], H. Tanaka[2], and T. Saito[2]

Advanced Science Research Center, Okayama University
[1]Neutron Therapy Research Center, Okayama University
[2]Institute for Integrated Radiation and Nuclear Science, Kyoto University

INTRODUCTION: The results of many previous radiation studies suggest that DNA is the primary target of radiobiological effects and that DNA damage is a major contributor to them. We have studied radiation-induced DNA damage. We have dealt not only with gamma- and X-rays, but also with heavy ion beams such as carbon ions, and have investigated whether DNA damage shows a specificity for the kind of radiation [1, 2]. In this research project, we have studied the characteristics of DNA damage caused by neutron radiation (see last year's report). This has been observed for DNA damage directly caused by neutrons, and from this year the characteristics of DNA damage species in BNCT (Boron Neutron Capture Therapy) will also be examined, because BNCT has had a predominant clinical application and much remains unknown about the molecular mechanisms of their cell death, i.e. the DNA damage modality. We here analyze the DNA damage caused by BNCT in cultured cells, in line with previous research methods.

EXPERIMENTS: Cultured cells of Chinese hamster ovary (CHO) strains with various DNA repair backgrounds were irradiated with neutron beams in the Kyoto University Reactor (KUR). The cells were cultivated with the conventional method. The logarithmic growing cells were recovered by trypsinization and the cells were mixed in BPA (L-4-Boronophenylalanine, Interpharma Praha, a. s, Czech) or BSH (Sodium mercaptododecaborate, Katchem spol. s. r. o., Czech) solution. The concentration of these chemicals was 25 μg mL^{-1} [3]. The mixture were set into polypropylene tubes for irradiation. The estimated dose rate of the neutron was 1 Gy h^{-1}. The irradiation periods were 0, 30, 60, 90, 120, 150 min. The irradiated cells were divided into two groups, one for viability and the other for DNA damage analysis by the same methods reported previously [4].

RESULTS: In this study, a slight decrease in survival and a slight increase in DNA damage were observed in the BPA- and BSH-treated groups compared to the untreated (control) group. DNA damage is viewed here as DNA double-strand breaks. This reduction in survival was not as dramatic as observed with usual BNCT treatment. This suggests that the BNCT drug treatment was inadequate in this study. The concentrations administered to the cells were each based on those previously reported [3], but the treatment time may have been too short. In the future study, we elongate the treatment time with BNCT drugs to increase the intracellular concentration by treating the cells from the time of cell culture.

REFERENCES:

[1] H. Terato *et al*., J. Radiat. Res., **49** (2008) 133-146.
[2] Y. Tokuyama *et al*., J. Radiat. Res., **56** (2015) 446-455.
[3] Y. Kinashi *et al*., Radiat. Oncol., **6** (2011) 106.
[4] H. Terato *et al*., KURNS Progress report 2022, (2023) 158.

CO6-20

Solution scattering study of of biomacromolecules depending on external environment

M. Shimizu, K. Morishima, R. Inoue, M. Sugiyama

Institute for Integrated Radiation and Nuclear Science, Kyoto University

INTRODUCTION: Most protein have unique tertiary structure depending on their amino-acid sequence. The tertiary structures are realized by various kinds of intra-molecule interactions, such as hydrogen bonding, salt bridge, etc. In addition, interaction between protein and surrounding water molecules are another important determinant of protein structures. Therefore, measuring dynamics of water molecules and other small molecules in the vicinity of protein surface is important for understanding protein structures. However, while computational modeling was reported [1], experimental methods to study the surrounding small molecules have not yet been established. We thought that a comparison of protein solution series with different osmolyte concentration would realize experimental analysis of the solvation environment, since osmolytes would change solvation state rather than tertiary structure of proteins.

EXPERIMENTS: We prepared three bovine serum albumin (BSA) solutions, which contain 0.1 M, 0.5 M, or 1.0 M betaine (FUJIFILM Wako Chemicals), respectively. The samples were prepared by dialyzing BSA standard (Thermo Fisher Scientific Inc.). Small-angle X-ray scattering was conducted for the aqueous solution of the BSA protein with the various concentration of betaine, using a NANOPIX (RIGAKU, Tokyo, Japan). Then radius of gyration was calculated from Guinier plot of the profiles. Analytical ultracentrifugation was also performed for the BSA samples by a ProteomeLab XL-I analytical-ultracentrifuge (Beckman Coulter). SAngler and SEDFIT were used for analysis [2, 3].

RESULTS: Guinier plots of the BSA solution are shown in Fig. 1. The radius of gyration for BSA solution with 0.1 M betaine, 0.5 M betaine, and 1.0 M betaine were, 28.8±0.2 Å, 28.9±0.2 Å, and 29.3±0.2 Å, respectively. Basically, the scattering profiles were similar each other. Nevertheless, a slight difference was observed between the radius of gyration of BSA solution with 0.1M betaine and that with 1.0M betaine. To examine whether the difference is assigned to difference in solvation state, oligomerization status of the BSA was investigated by analytical ultracentrifugation. As a result, the fraction of monomeric BSA was 98.9%, 96.7%, and 94.7% for the solution containing 0.1 M betaine, 0.5 M betaine, and 1.0 M betaine, respectively. The results suggest that the difference in the radius of gyration is mainly caused by difference in contents of oligomeric BSA. In conclusion, these experiments demonstrate that it is difficult to solvation state of biomolecules only from small-angle X-ray scattering because a series sample that differs only in the solvation cannot be prepared.

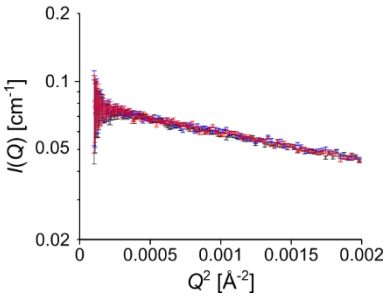

Figure 1. Guinier plots of BSA proteins for various betaine concentrations. The profile at 0.1 M betaine is shown by black open circle, that at 0.5 M betaine is shown by blue open square, and that at 1.0 M betaine is shown by red open triangle, respectively. The error bars show standard deviations.

REFERENCES:

[1] D. Nerukh, *et al.,* J. Phys. Chem. Lett. **3** (2012) 3663–3664.
[2] N. Shimizu, *et al.*, AIP conf. Proc., **1741** (2016).
[3] P. Schuck, Biophys. J., **78** (2000)1606-1619.

CO6-21

Neutron activation of gold nanoparticles for future theranostics

A. Toyoshima, N. Koshikawa[1], Y. Kadonaga, Y. Kikuchi[1], K. Tokoi[2], H. Kato, K. S. Tanaka[1], and J. Kataoka[1]

Institute for Radiation Sciences, Osaka University
[1]Graduate School of Advanced Science and Engineering, Waseda University
[2]Graduate School of Science, Osaka University

INTRODUCTION: Gold nanoparticles (AuNPs) are promising drug carriers, and its visualization is essential because various factors, such as their size and shape, can change its biodistribution. However, methods to visualize AuNP directly and with high sensitivity has not yet been established. Therefore, we propose activation imaging of AuNP[1]. When gold nanoparticles are irradiated with neutrons, stable ^{197}Au becomes radioactive ^{198}Au (half-life: 2.7 days), which predominantly emits 412-keV gamma rays that allows imaging. In this study, neutron-activated AuNP, [^{198}Au]AuNP, was synthesized, injected to the tumor-bearing mice, and visualized by wide-band X-rays/gamma-ray imager, hybrid Compton camera (HCC)[2]. Moreover, we labeled the alpha-emitting therapeutic drug, ^{211}At, on the [^{198}Au]AuNP and demonstrated in-vivo imaging.

EXPERIMENTS: We first synthesized [^{198}Au]AuNP with [^{198}Au]$HAuCl_4$ and $NaBH_4$ as a reductant. After purification of [^{198}Au]$HAuCl_4$ by ultrafiltration, surface-modification of [^{198}Au]$HAuCl_4$ was performed with mPEG(5k)-SH. Synthesized [^{198}Au]AuNP-S-mPEG(5k) was finally purified by ultrafiltration. We injected 0.3 MBq of [^{198}Au]AuNP to the mice intratumorally and visualized with HCC. Moreover, [^{198}Au]AuNP-S-mPEG(5k) was quantitatively astatinated. We injected [^{211}At/^{198}Au]AuNP-S-mPEG(5k), which is 0.2 MBq as ^{198}Au and 0.7 MBq as ^{211}At, intravenously to the mice. Subsequently, imaging was performed with HCC.

RESULTS: As shown in Fig. 1, [^{198}Au]AuNP in the tumor of the mouse was clearly visualized 9 minutes and 4 days after the injection. Spread of the accumulation observed in the image obtained 4 days after the injection may indicate the migration of the AuNP from the tumor to other organs. Fig. 2 shows the images of the mice injected with [^{211}At/^{198}Au]AuNP. (a-1) and (a-2) are the distribution of ^{211}At obtained using 79-keV X-rays 9 minutes and 2 days after the injection, and (b-1) and (b-2) are the distribution of ^{198}Au obtained using 412-keV gamma rays 9 minutes and 2 days after the injection. Simultaneous imaging of ^{211}At and ^{198}Au was demonstrated by the images (a-1) and (a-2). Moreover, 2.7-days half-life of ^{198}Au allowed the long-term visualization of drugs even after visualization of ^{211}At became impossible 2 days after the injection because of its short half-life (7.2 hours).

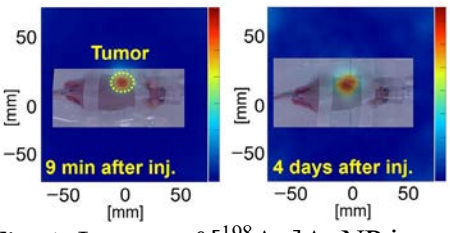

Fig. 1. Images of [^{198}Au]AuNP intratumorally injected to the mouse.

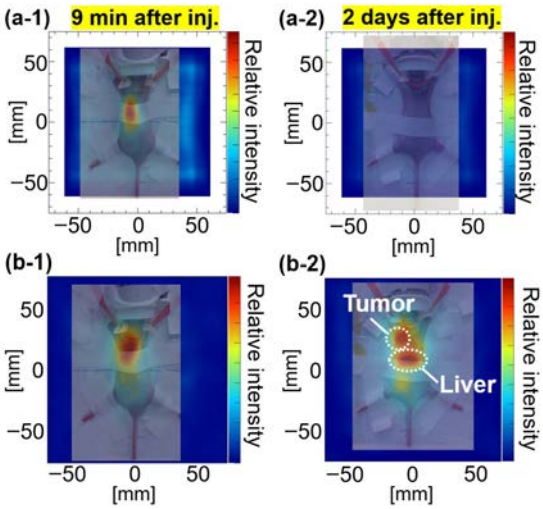

Fig. 2. Images of [^{211}At/^{198}Au]AuNP intravenously injected to the mouse. ^{211}At (a-1) and ^{198}Au (b-1) 9 min after injection, ^{211}At (a-2) and ^{198}Au (b-2) 2 days after injection.

REFERENCES:

[1] N. Koshikawa *et al.*, Nucl. Instr. and Meth., A, **1045** (2023) 167599.
[2] A. Omata *et al.*, Sci. Reports, **10** (2020) 14604.

CO6-22

Structural study of water-soluble vitamin K_2 from *Bacillus subtilis natto*

T. Chatake, A. Okoda, K. Morishima, R. Inoue, M. Sugiyama, T. Takata, Y. Yanagisawa[1]

Institute for Integrated Radiation and Nuclear Science, Kyoto University
[1]Faculty of Pharmacy, Chiba Institute of Sciences

INTRODUCTION: Natto is one of the popular traditional Japanese foods made from soybeans fermented by *Bacillus subtilis natto* (BSN). BSN produce several kinds of bioactive substances, vitamin K_2 [1], nattokinase [2], dipicolinic acid, and so on. Interestingly, BSN produce a water-soluble complex of menquinone-7, which is a kind of vitamin K_2, and peptides [3]. In our previous studies, the water-soluble complex (hereafter called *natto*-MK-7) was highly purified from the liquid medium of BSN, and its size was estimated by dynamic light scattering [4]. In addition, peptides in *natto*-MK-7, called K-binding factor (KBF), were investigated by MALDI-TOF mass spectrometry (MALDI-TOF MS) and amino acid analysis [5]. Recently, KBF was extracted and purified by HPLC. The latest results are presented here.

EXPERIMENTS: *Natto*-MK-7 was extracted from the liquid culture medium of BSN and purified by fast protein liquid chromatography [4]. KBF was isolated from *natto*-MK-7 by *reversed-phase high performance liquid chromatography* (RP-HPLC). This liquid chromatography was performed by isocratic elution with 0.1% TFA in acetonitrile using a C18 column. Two peaks were collected, and the molar mass of peak containing each peptide was confirmed by MALDI-TOF MS.

RESULTS: Two peaks were observed at 41.8 and 43.2 min in RP-HPLC of *natto*-MK-7, as shown in Fig. 1. The two peaks correspond to KBF in *natto*-MK-7. Fig. 2 shows the MALDI-TOF MS spectrum of *natto*-MK-7 before RP-HPLC, and 41.8 min and 43.2 min fractions of RP-HPLC. They show significant peaks between m/z = 1,020 ~ 1,100, indicating the molecular weight of KBF. MALDI-TOF MS and amino acid analysis of *natto*-MK-7 suggested that KBF were the various combinations of nine amino acids, including Asx, Glx, Val, Leu, and Met (Asx: Asp or Asn, Glx: Glu or Gln). The 41.8 min and 43.2 min fractions had the different combinations of peaks at m/z = (1030.4, 1062.6, 1066.4, 1076.4 and 1080.4) and (1044.4, 1058.5, 1062.6 and 1076.4), respectively. In conclusion, the present RP-HPLC could isolate and separate the KBF into two groups.

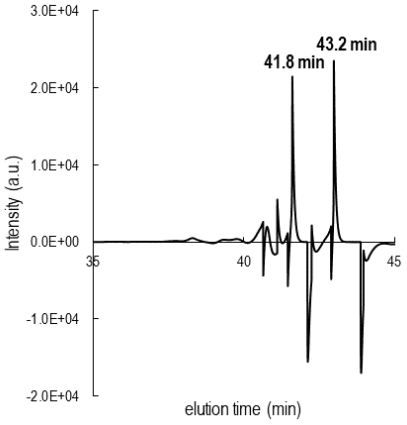

Fig. 1. The chromatography charts of RP-HPLC of *natto*-MK-7.

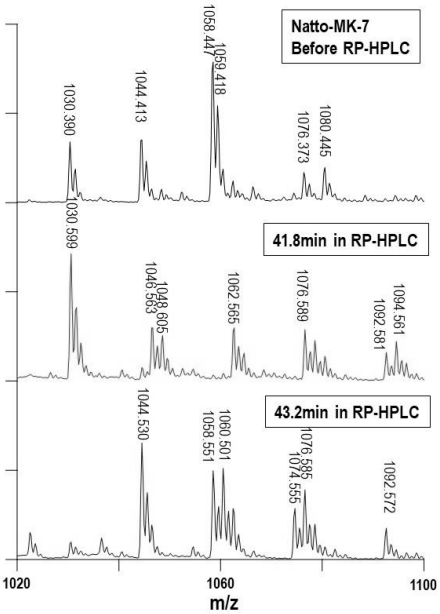

Fig. 2. The MALDI-TOF MS spectrum of *natto*-MK-7, KBFs (41.8 and 43.2 min).

REFERENCES:

[1] L. Wen *et al.*, Mol. Med. Rep., **18**, (1999) 3-15.
[2] (a) H. Sumi *et al.*, Experientia, **43** (1987) 1110-1111.
(b) Y Yanagisawa *et al.*, J. Synchrotron Rad., **20** (2013) 875–879.
[3] H. Ikeda, Y. Doi, Eur. J. Biochem., **192**, (1990) 219-224.
[4] T. Chatake *et al.*, J. Food Biochem., (2018) e12630.
[5] T. Chatake *et al.*, J. Biochem., **174** (2023) 383-389.

CO6-23

Distribution analysis of the chemical modification of the amino acid residues in mice lens structural proteins during age-related cataract

S. Matsushita[1], A. Nakamura[1], Y. Suzuki[1] and T. Takata[2]

[1] *Dept of Materials and Applied Chemistry, Nihon University*
[2] *Institute for Integrated Radiation and Nuclear Science, Kyoto University*

INTRODUCTION: Age-related cataracts are the leading causes of blindness in world. Several risk factors, contributing to the development of cataracts, have been reported. Above all, abnormal lens protein aggregation and insolubilization has been believed as the main process. Alteration of lens protein structure, caused by covalently post-translational modifications, are thought to be critical for maintaining lens protein homeostasis [1]. We have shown that covalent modifications of amino acid residues as a scale for a lens aging. To do this, mass spectrometry is an efficient tool to quantitative analysis, however the distributions of modifications were very obscured. Therefore, we are to address revealing the distribution of modifications (isomerization of Asp) in the lens section using by Imaging Mass Spectrometry (IMS) [2]. This technique requires the preparation of high-quality sections, but we could not have prepared the samples available for IMS so far. Since it has been very difficult to attach water-rich lens tissues to analytical glass plate, we tried to spray lens model peptide for the sample plate for analysis.

EXPERIMENTS: We constructed a system to make uniformed spraying sample plate for IMS, which was coated by a chemically synthesized peptide (Fig. 1). Then, we synthesized model peptide containing a site where isomerize Asp has been detected in crystallin, which serves as a lens model. The modification was confirmed using by LC-MS systems in Institute for Integrated Radiation and Nuclear Science, Kyoto University (data not shown). Next, we tried to purify the enzyme to cleave D-Asp in peptide/protein. This is because of that to obtain subtracted MS images before digestion and after digestion. In order to get pure enzyme, we used his-tag systems and then cleaved his-tag after purification.

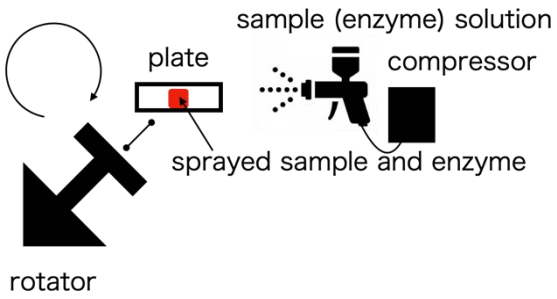

Fig. 1. The schematic drawings for uniformed spraying samples/enzyme into glass plate.

RESULTS: The uniformed spraying system for samples/enzyme was constructed (Fig. 1). This system would help to optimize sample preparation for obtaining ideal images for IMS. We also obtained protease for D-Asp containing peptide/protein. The purity of enzyme was confirmed by SDS-PAGE (Fig. 2). Since the size of enzyme was smaller than those from amino acid sequence data, some degradation/truncation would be occurred under current situation. To the end, we success to obtain the optimized system, samples and specific enzyme for this study. After check the activity of this enzyme, we will use all for IMS systems.

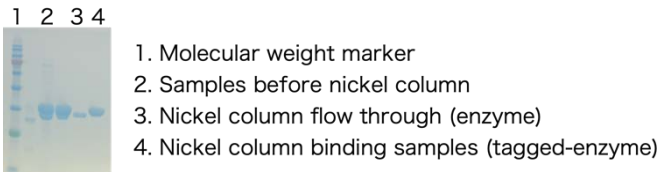

Fig. 2. The purification of enzyme that specific digestion of D-Asp containing peptide/protein.

REFERENCES:

[1] N. Fujii *et al.*, Biochim. Biophys. Acta, **1860** (2016) 183-191.
[2] J. McMahon *et al.*, J. Am. Soc. Mass. Spectrrom., **11** (1995) 1047-1058.

CO6-24

Molecular dynamics analysis of oxidative folding enzyme ER-60 with solution scattering measurement

A. Okuda, M. Shimizu, K. Morishima, R. Inoue, R. Urade and M. Sugiyama

Institute for Integrated Radiation and Nuclear Science, Kyoto University

INTRODUCTION: ER-60, an oxidative protein folding enzyme, is a multi-domain protein. ER-60 has **a** and **a'** domains with catalytically active cysteine pairs and **b** and **b'** domains in the order **a**-**b**-**b**-**b'**-**a'**. In the process of oxidative protein folding, ER-60 might have the appropriate domain conformations to function, and it is estimated that the structure fluctuates and changes according to the redox state of active cysteine pairs in the solution [1]. Neutron scattering measurement takes advantage of the large difference in neutron scattering length between hydrogen and deuterium, is useful for observing the dynamics and structures of such multi-domain proteins, ER-60 in solution. When 75% deuterated and hydrogenated proteins are in 100% deuterated solvent, the deuterated proteins are scatteringly invisible, and only the hydrogenated proteins could be observed. Applying this method to multi-domain proteins, the domain of the hydrogenated domains could be selectively observed. To reveal the structure-function correlations of ER-60, we aim to analyze selective domain dynamics by quasi-elastic neutron scattering (QENS). The segmental deuterated proteins for this experiment were prepared by connecting the domains with the ligation enzyme *Oa*AEP [2].

EXPERIMENTS: The 75% deuterated (*d*) and hydrogenated (*h*) domains were expressed in *E. coli* cultured in M9 medium containing 75% deuterium and LB medium without deuterium, respectively [3]. The purified domains were mixed in buffer containing 200 mM Tris-HCl (pH 7.4) / 150 mM NaCl. Then, 0.2 μM of the ligation enzyme *Oa*AEP was added to the mixture, and the protein ligation reaction was performed at 20°C for 64 hours. The results of ligation reactions were confirmed by SDS-PAGE. SAXS measurements were performed at 25 °C with 4 hours of exposure-time using a NANOPIX (Rigaku, Tokyo, Japan). The sample-to-detector distance was set to 1330 mm and 300 mm. The q range was from 0.01 to 0.80 Å $^{-1}$.

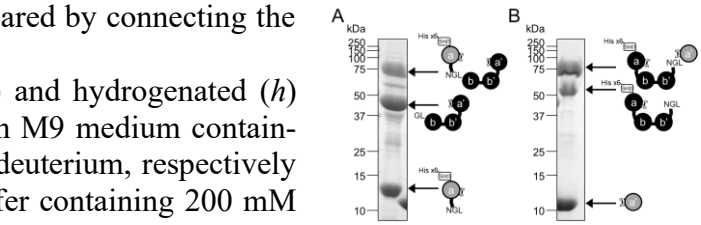

Fig. 1. The ligation products from (A) (*h*)**a** and (*d*)**bb'a'** domains and (B) (*d*)**abb'** and (*h*)**a'** domains of ER-60 by *Oa*AEP.

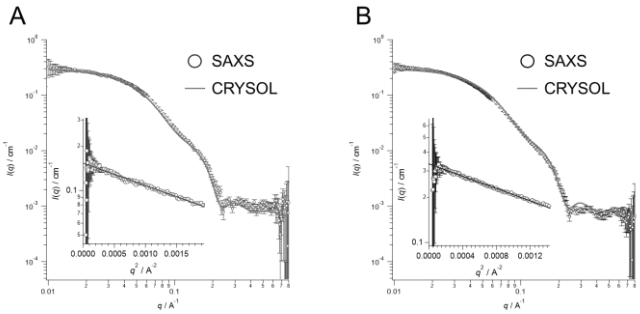

Fig. 2. The SAXS profiles of (A) (*h*)**a**-(*d*)**bb'a'** and (B) (*d*)**abb'**-(*h*)**a'** of ER-60. the radius of gyration (R_g) of these are 32.2 ± 0.3 Å and 37.3 ± 0.2 Å, respectively. Inset panels are guinier plots of them.

RESULTS: The band of ligation product, (*h*)**a**-(*d*)**bb'a'** and (*d*)**abb'**-(*h*)**a'**, connecting the deuterated and hydrogenated domains were observed, indicating the progress of the protein ligation reaction (Fig. 1). In the SAXS profiles of (*h*)**a**-(*d*)**bb'a'** and (*d*)**abb'**-(*h*)**a'** (Fig. 2), there were no significant differences from the profiles predicted by CRYSOL [4] from the crystal structure, and no structural disruption occurred. However, R_g of **abb'**-(*h*)**a'** was larger than predicted, suggesting the possibility of aggregations. Currently, we are examining the conditions for obtaining the stable samples.

REFERENCES:

[1] A. Okuda *et al.*, Sci Rep., **11** (2021) 5655.
[2] A. Okuda *et al.*, Angew Chem Int Ed Engl., **62** (2023) e202214412.
[3] A. Okuda *et al.*, Biophys Physicobiol., **18** (2021) 16-27.
[4] D. Franke *et al.*, J. Appl. Cryst., **50** (2017) 1212-1225.

CO6-25

Synthesis and evaluation of BPA-Nitroimidazole conjugates as smart drug for treatment of hypoxic cells

K. Tanabe,[1] T. Nishihara,[1] T. Ozasa[1] and M. Suzuki[2]

[1]*Department of Chemistry and Biological Science, College of Science and Engineering, Aoyama Gakuin University*
[2]*Institute for Integrated Radiation and Nuclear Science, Kyoto University*

INTRODUCTION: The fast and accurate treatment of hypoxic regions in living tissue is critical for medical treatment of solid tumor, because it has been associated closely with the malignant phenotype of cancer cells, resistant to cancer therapies and the high mortality rate of cancer patients.[1] For treatment of tumor hypoxia, a considerable number of studies have been conducted over the past few decades on the development of radiosensitizers and prodrugs for treatment of tumor hypoxia. However, estimation of treatment method for this pathological tissue remains inadequate, and there are increasing demands for a convenient protocol for its treatment.

These research contexts prompted us to prepare a novel drug that could be used to treat hypoxic cells and tumor hypoxia by BNCT. We conjugated drug for BNCT, BPA, with 2-nitroimidazole derivatives (NIs) to form new hypoxia-treating drug (BPA-NI, Fig 1). NIs are known as an exogeneous marker for hypoxia because of its characteristic reactions in hypoxic cells. NIs are selectively reduced by nitroreductase under hypoxic conditions to form reactive products that can irreversibly bind to cellular nucleophiles. Ultimately, the binding of NIs to cellular macromolecules leads to their accumulation in hypoxic cells and regions. In this study, we prepared the BPA-NI and characterized its cytotoxic effects upon thermal neutron irradiation.

EXPERIMENTS:

Cellular experiments using BPA-NI. The BPA-NI (0 or 250 μM) was administered to the SAS cells and then the cells were incubated for 3 h. After incubation and wash, the cells were irradiated (neutron, 1 MW) for 45 min at KUR. After incubation, WST 8 was added to the cells, and the cell viability assay was performed using Microplate Reader.

RESULTS: The Huisgen reaction was utilized to introduce the NI group into BPA: a benzyl azide group was introduced into the amino group of BPA, which was then condensed with the acetylene group of the NI group in the presence of a copper catalyst. The resulting BPA-NI was identified using NMR and MS spectra.

Next, the cytotoxic effect of neutron irradiation with BPA-NI was evaluated. BPA-NI was administered to human squamous cell carcinoma cells SAS and cultured under hypoxic or aerobic conditions. Subsequent irradiation with thermal neutron beams showed a high cell-killing effect in hypoxic cells, while the effect was limited in aerobic cells. These results strongly indicate that BPA-NI selectively accumulated in hypoxic cells due to the effect of NI substituent and showed toxicity under irradiation conditions. Thus, we successfully developed novel drug for hypoxic cells. The in vivo experiments for evaluation of cytotoxic effects of BPA-NI is in progress.

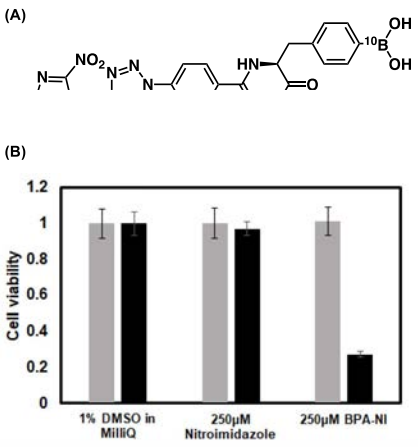

Fig. 1. (A) Chemical structure of BPA-NI. ((B) Cytotoxic effect of BPA-NI and control compound 2-nitroimidazole with (black) or without (gray) thermal neutron irradiation.

REFERENCES:

[1] Harris, A. L., Nat. Rev. Cancer, **2** (2002) 38.

CO6-26

Evaluation of fluorodeoxyuridine derivative bearing azide-methyl substituent as prodrug for FLASH-RT

K. Tanabe,[1] T. Nishihara,[1] T. Ozasa[1] and M. Suzuki[2]

[1]*Department of Chemistry and Biological Science, College of Science and Engineering, Aoyama Gakuin University*
[2]*Institute for Integrated Radiation and Nuclear Science, Kyoto University*

INTRODUCTION: Radiation therapy (RT) is known as a major treatment modality in cancer therapy and is widely used. However, its application in the treatment of tumors that exhibit radioresistance remains limited by dose-limiting normal tissue complications. Under these circumstances, FLASH-RT has been attracting attention. FLASH-RT is an ultrafast RT with dose rates that are generally thousands of times higher than those currently used in routine clinical practice. A major advantage of FLASH-RT is that when irradiated to living tissue, normal tissue is protected compared to conventional RT. These research contexts prompted us to design smart drugs which are applicable to FLASH-RT.
Here we discuss an application of radiation-activated prodrug of antitumor agent, 5-FdUrd, with an azidomethyl group (N3-FdUrd),[1] a known substituent that can be desorbed under X-irradiation conditions. We expected that N3-FdUrd would be activated by reducing species generated by radiolysis (Figure 1), which would remove azide methyl unit to give 5-FdUrd. We prepared the N3-FdUrd and assessed the radiation-dependent cytotoxicity of N3-FdUrd using living cells.

EXPERIMENTS:
Cellular experiments using N3-FdUrd. The N3-FdUrd (0 or 10 μM) was administered to the A549 cells and then the cells were incubated for 24 h. After incubation and wash, the cells were irradiated (0 or 20 Gy) under normoxic conditions using KURNS-LINAC. After incubation, WST 8 was added to the cells, and the cell viability assay was performed using Microplate Reader.

RESULTS: N3-FdUrd was prepared according to the previous report.[1] Next, we attempted to test the cytotoxic effects of N3-FdUrd by irradiating A549 cells under normoxic conditions in the presence or absence of N3-FdUrd to characterize the radiation-dependent cytotoxic effects of N3-FdUrd. As shown in Figure 1B, the cells were viable even in the presence of 10 μM N3-FdUrd without irradiation. On the other hand, radiation in the presence of N3-FdUrd significantly enhanced the radiation sensitivity of the A549 cells, resulting in low cell viability. When the concentration of N3-FdUrd was changed, higher concentrations of N3-FdUrd showed higher cell-killing effects, suggesting that prodrug activation is involved in the enhancement of cell-killing effects by irradiation. These results strongly indicate that N3-FdUrd released toxic 5-FdUrd by radiolytic reduction in hypoxic cells, which led to enhanced cytotoxicity.

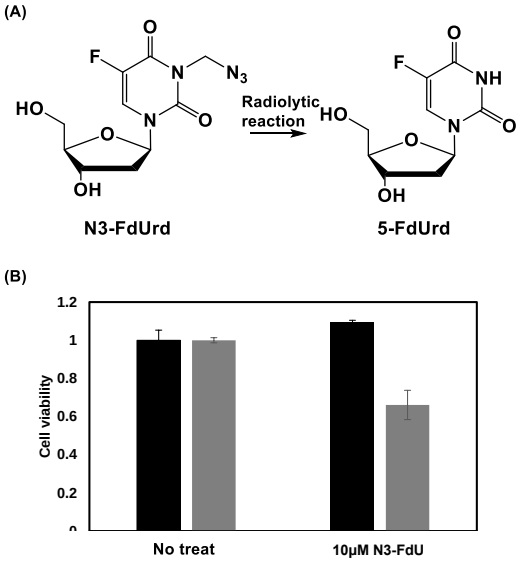

Fig. 1. (A) Radiolytic reaction of N3-FdUrd to form 5-FdUrd. ((B) Cytotoxic effect of N3-FdUrd with or without irradiation (0 Gy: black, 20 Gy: gray).

REFERENCES:
[1] Tanabe, K.; Ishizaki, J.; Ando, Y.; Ito, T.; Nishimoto, S., Bioorg. Med. Chem. Lett., **22** (2012) 1682.

CO6-27

N-Acetylneuraminic Acid Functioned as the Scavenger for Reacive Oxygen Species

N. Fujii and T. Takata[1]

Radioisotope Research Center, Teikyo University
[1] Institute for Integrated Radiation and Nuclear Science, Kyoto University

INTRODUCTION: *N*-Acetylneuraminic acid (Neu5Ac) is a sialic acid in mammals, certain mollusks and some microorganisms. The Neu5Ac was found with a capping sugar in the oligosaccharide chains of glycoproteins and glycolipids [1]. Most studies on glycanic Neu5Ac have focused primarily on cell protection, fertilization, immunology, inflammation and tumors [2-4]. Free Neu5Ac molecules is well oxidized by H_2O_2, then produce its decaroxy product, 4-(acetylamino)-2,4-dideoxy-D-glycero-D-galacto-octonic acid (ADOA) [5]. As a result, monomeric Neu5Ac is the potent defense molecule against oxidative damage. In this study, we used ionizing radiation for decomposing water to generate various reactive oxygen species (ROS), then the scavenged ROS by Neu5Ac was screened.

EXPERIMENTS: Nu5Ac, Ascorbic acid (Asc), Glutathione (GSH), Catalase and Superoxide dismutase (SOD) were dissolved in water, and the pH of the solution was adjusted to about 7.0 with sodium hydroxide. Gamma-irradiation was carried out at the Co-60 Gamma-ray Irradiation Facility of the Kyoto University Institute for Integrated Radiation and Nuclear Science. Sample aqueous solutions were irradiated with gamma ray at a dose of 1 kGy. The quantitative analysis of ADOA was used by LC-MS/MS. The high-performance liquid chromatography was used a U3000HPLC system (Thermo Fisher scientific). The mass spectrometer was used Q Exactive (Thermo Fisher scientific). ADOA was measured by parallel reaction monitoring (PRM) in the positive ion mode, using transitions m/z 282.11 → m/z 186.07.

RESULTS: To quantitatively investigate the amount of ADOA, PRM method was set the optimal for commercial standard. Fig. 1 show the production of ADOA from Neu5Ac aqueous solution with the addition of various scavengers for samples. The 1 kGy gamma-ray irradiation for 10 mM Neu5Ac solution increased the ADOA amount to about 140 μM (Fig. 1: control). Asc and GSH partially suppressed some amounts of ADOA, indicated the presence of the hydroxyl radical (·OH). Catalase suppressed the formation of ADOA completely at 10 U, but SOD did not at the same concentration. Those data implied the presence of hydroxyl radical and hydrogen peroxide, but major source of ADOA would be the hydrogen peroxide in sample after irradiation by gamma-ray.

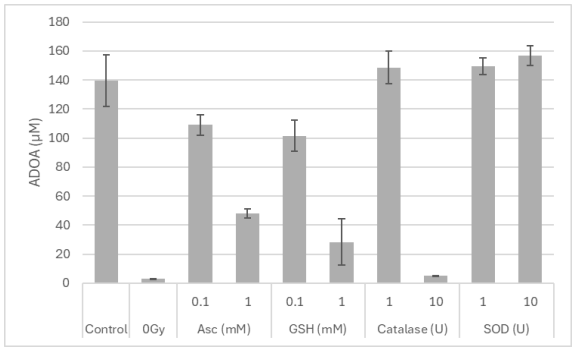

Fig. 1. The amount of ADOA in the presence of various scavengers**.**

REFERENCES:

[1] R. Schauer R., Zoology, **107** (2004) 49-64.
[2] T. Angata *et al.*, Chem. Rev., **102** (2002) 439-469.
[3] R. P. Crocker, Curr. Opin. Struct. Biol., **12** (2002) 609-615.
[4] K. Takayama *et al.*, Proc. Natl. Acad. Sci. USA **93** (1996) 10662-10667.
[5] R. Iijima *et al.*, FEBS Lett., **561** (2004) 163-166.

CO6-28

^{11}C Medical-isotope Production via ^{12}C(γ,n)^{11}C Reaction with Single-walled Carbon Nanotubes

N. Takahashi[1,2], M. Kurosawa[1], M. Tamura[1], M. Fujiwara[1,2], T. Kubota[3], N. Abe[4], and T. Takahashi[4]

[1]*Research Center for Nuclear Physics, Osaka University*
[2]*Kyoto Medical Technology*
[3]*Agency for Health, Safety and Environment, Kyoto University*
[4]*Institute for Integrated Radiation and Nuclear Science, Kyoto University*

INTRODUCTION: L-[^{11}C]-Methionine is used as a positron emission tomography (PET) reagent for medical diagnosis of brain tumors [1]. The medical ^{11}C radioisotopes are mostly produced in a cyclotron via the ^{14}N(p,α)^{11}C reaction by bombarding enriched nitrogen gas with a proton beam [2]. Instead of producing ^{11}C with the cyclotron, we developed a novel method of producing ^{11}C using the bremsstrahlung γ-rays with a single-walled carbon nanotubes (SWCNT) to get a reasonable number of the ^{11}C activity.

EXPERIMENTS: Figure 1 shows the experimental scheme for the ^{11}C production via the ^{12}C(γ,n)^{11}C reaction. Bremsstrahlung γ-rays were produced by impinging a 40 MeV electron beam on platinum converter at the electron LINAC facility. The γ-rays were irradiated to SWCNT sealed in aluminum vessel with non-woven masks as gas inlet/outlet filter. The produced ^{11}C inside the vessel were oxidized to ^{11}CO or ^{11}CO$_2$ in O$_2$ gas, which was continuously flown during the irradiation. The ^{11}C gas (^{11}CO and ^{11}CO$_2$) were trapped in two 13X molecular sieve columns and 511-keV γ-rays from positron-electron annihilation were detected with CdZnTe detectors. The SWCNT with a diameter of 2-3 nm were used as target.

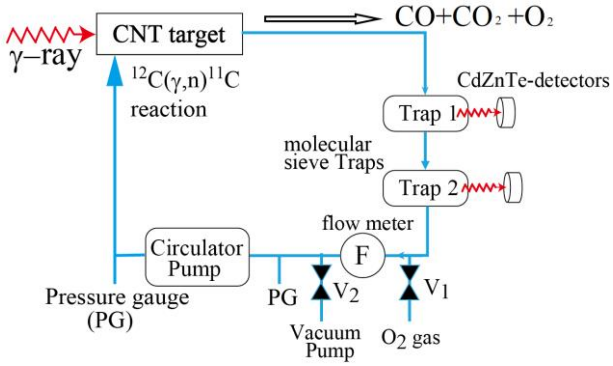

Fig. 1 Experimental scheme to produce ^{11}C and measure the extraction rate of ^{11}C gas.

RESULTS: Table 1 shows the normalized activity of ^{11}C gas for SWCNT which have different bulk density. The normalized activity slightly increases as bulk density increased. All the values shown in Table 1 are higher than 8.71 kBq/μA/g/min for SWCNT with a diameter of 1-1.4 nm used in the previous experiments.

Based on the experimental production rate of ^{11}C gas, we estimate that we can obtain the ^{11}C activity of 58 GBq when we use a SWCNT target under the conditions with 1) a length of 50 cm, 2) weight of 1.13 kg for 0.155 g/cm^3, 3) a 40 MeV electron beam intensity of 100 μA for 40 minutes bombardment.

Table 1 Normalized activity of ^{11}C gas for each bulk density

Bulk density of SWCNT (mg/cm^3)	Normalized activity of ^{11}C gas (kBq/μA/g/min)
3.27	13.30±0.07
6.53	13.94±0.07
9.80	14.41±0.06
13.06	14.92±0.05

REFERENCES:

[1] Kobayashi K. *et al.*, Eur. J. Nucl. Med. Mol. Imaging, **42** (2015) 1071-1080.
[2] David R. Christman *et al.*, Int. J. appl. radiat. isot., **26** (1975) 435-442.

CO6-29

Fundamental study for the production of radionuclide endohedral fullerenes using an infrared fiber laser

M. Inagaki, H. Nakada[1], S. Sekimoto and T. Ohtsuki

Institute for Integrated Radiation and Nuclear Science, Kyoto University
[1]Graduate School of Engineering, Kyoto University

INTRODUCTION: Radioactive isotopes (RI) are widely used in medical diagnosis and treatment. To utilize RI for diagnosis and treatment, techniques for transporting RI in the body and accumulating it at the affected site, known as drug delivery systems (DDS), are required. Fullerene, due to its cage-like structure capable of encapsulating metal atoms, etc. [1], can serve as a molecule for DDS if it is chemically modified to possess functionality to accumulate at the affected site. Therefore, this study aimed to develop a simple method for generating fullerene encapsulating RI.

EXPERIMENTS: (1) Graphite was placed in a quartz vessel, and the vessel was purged with argon gas at 50 kPa. Laser irradiation was applied to the sample from the outside of the vessel. The laser used was a continuous-wave fiber laser with a wavelength of 1080 nm and a power of 300 W. After irradiation, o-dichlorobenzene (*o*-DCB) was added to the sample, and the soluble components were extracted and analyzed by HPLC.
(2) Graphite (70 mg) and radioactive CeO_2 (8 mg) were placed in a quartz vessel, and laser irradiation was conducted under the same conditions. The radioactive CeO_2 was produced using the electron linear accelerator of the Institute for Integrated Radiation and Nuclear Science, Kyoto University. After irradiation, *o*-DCB was added to the sample, the soluble components were extracted, filtered through a membrane filter, and then gamma-ray measurements were performed using a Ge semiconductor detector. Subsequently, similar extractions were performed using aniline and pyridine, followed by gamma-ray measurements.

RESULTS and DISCUSSION: The results of HPLC are shown in Figure 1. From the HPLC results, it was found that fullerenes of C_{60}, C_{70}, and higher fullerenes such as C_{84} were successfully generated by this method. Gamma-ray measurement results of *o*-DCB, aniline, and pyridine solutions obtained from the RI-encapsulating fullerene generation experiment are presented in Table 1. Gamma rays originating from ^{139}Ce and ^{141}Ce were observed more strongly in the aniline and pyridine solutions than in the *o*-DCB solution. Since CeO_2 is insoluble in *o*-DCB, aniline, and pyridine and does not pass through the membrane filter, this result indicates that a component containing ^{139}Ce and ^{141}Ce, insoluble in *o*-DCB but soluble in aniline and pyridine, was formed. Further work will be done to identify this component.

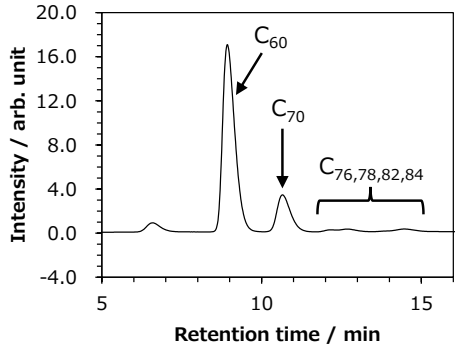

Fig. 1. Chromatogram obtained by HPLC.

Table 1. Gamma-ray measurement results.

solvent	Gamma ray intensity / cps	
	^{139}Ce	^{141}Ce
o-DCB	0.26	0.08
Aniline	0.96	0.30
Pyridine	1.74	0.55

REFERENCES:
[1] Y. Chai *et al.*, J. Phys. Chem., **95** (1991) 7564–7568.

CO6-30

Screening for substances that inhibit abnormal protein aggregation

H. Yagi[1] Y. Kagasawa[2] and T. Takata[2]

[1] *Faculty of Engineering, Tottori University*
[2] *Institute for Integrated Radiation and Nuclear Science, Kyoto University*

INTRODUCTION: Cataract, Alzheimer's disease, Parkinson's disease, and prion disease are diseases that share a common basis in abnormal protein aggregation and typical fibrosis. However, the cause of protein aggregation/fibrosis has been very obscured, and the pathogenesis of these diseases has not yet been elucidated. *In vivo*, accumulation of large amounts of protein aggregates has been observed at disease-causing sites. Therefore, one way to control disease would suppress the formation of abnormal protein aggregates. To do that, the important factor for successful screening of inhibitors is the establishment of monitoring system with a simple and reproducible mechanism of protein aggregation. In past years, we have used γ-ray irradiation to artificially create abnormal protein folding products [1]. We produce recombinant human βB2-crystallin, one of the human lens component proteins by *E. coli*. This protein can be completely denatured with various stresses or chemicals, but then refolded by rapid dilution under appropriate conditions. In this study, we irradiated βB2-crystallin to induce abnormal chemical modification of amino acid residues in it, then monitored refolding process using their intrinsic native tryptophan fluorescence. The purpose of this study is to develop monitoring systems for screening small molecules affecting folding/misfolding pathway of proteins.

EXPERIMENTS: Material Recombinantly expressed human lens βB2-crystallin was prepared and purified as described previously [2]. 1.0 mg/mL aliquots of βB2-crystallin in phosphate buffered saline solution were flash frozen in liquid nitrogen and stored at −80 °C until use. Irradiation was carried out at the $_{60}$Co Gamma-ray Irradiation Facility of the Kyoto University Institute for Integrated Radiation and Nuclear Science [1]. Irradiated samples were centrifuged then collected supernatant. The concentration of βB2-crystallin was measurements by BCA assay kit (ThermoFisher). Unfolding of βB2-crystallin was performed by using 6 M Urea. Refolding was initiated by rapid dilution in ten times of the same buffer in the absence of urea [3].

RESULTS: The amount of βB2-crystallin was decreased in the water-soluble fraction as a function of irradiation dose (Fig. 1). The amount of unfolding/refolding of βB2-crystallin was observed in native fluorescence with some decreasing peak intensity even after low dose (~5 Gy) irradiated (Fig. 2). In independent experiment, we identified that irradiation induces oxidization of five tryptophan residues in βB2-crystallin. This would impact the current folding/misfolding monitoring system. Further improvements of current monitoring systems are required, based on the reduction in fluorescence intensity due to modification.

Fig.1. Aggregates of βB2-crystallin after irradiation.

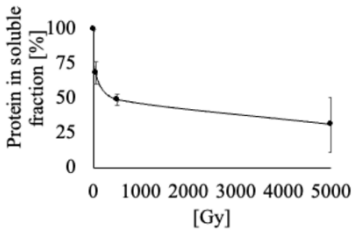

Fig.2. Monitoring of refolding process of low dose (~5 Gy) irradiated βB2-crystallin.

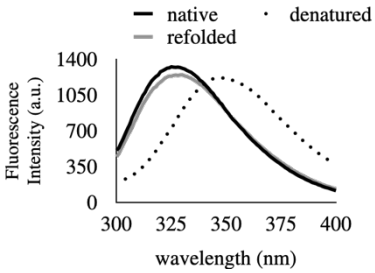

REFERENCES:

[1] I. Kim *et al.*, Amino Acids., **48** (2016) 2855-2866.
[2] T. Takata *et al.*, Mol Vis., **15** (2009) 241-249.
[3] T. Takata *et al.*, FEBS J., **285** (2018) 2263-2277.

CO6-31

Elucidating the Molecular Basis for the Increased Risk of Nuclear Cataract Development with Global Warming

N. Yamamoto[1] and T. Takata[2]

[1] *Fujita Health University*
[2] *Institute for Integrated Radiation and Nuclear Science, Kyoto University*

INTRODUCTION: The transparency of the lens is important for focusing target onto retina. Lens cells contain rich stable long-lived structural proteins, which is called as crystallin. Recently, the worldwide epidemiological survey confirmed that the risk of nuclear cataract (NUC) is significantly higher in residents living in areas where the annual number of days with temperatures of 30°C or higher is higher. Furthermore, in an *in silico* simulation study, the applicant group showed that the incidence of NUC differs within a range of internal temperature differences (35.0-37.5°C) [1]. Based on these results, this study aims to clarify the relationship between the formation of NUC and temperature. There were also significant changes in cell proliferation and expression of crystallins during the process, indicating that temperature-dependent changes occur during protein biosynthesis inside the cell. After reviewing these results, we came to the hypothesis that there is a temperature dependence in the crystallin folding pathways inside the cell, and decided to conduct the following study to demonstrate temperature dependent different folding pathway *in vitro*.

EXPERIMENTS: Recombinantly expressed human βB2-crystallin was unfolded, then refolded by dilution in the presence of each concentration of urea. The ratio of fluorescence intensities between folded (320 nm) and unfolded (360 nm) states were used for the folding index under various urea concentration. This refolding experiment was performed under at two different temperature environment (35.0 vs 37.5°C). On the other hand, a mutant (Trp59Cys) was also prepared as a model for hereditary NUC development, but it was difficult to express under 37 °C because of that aggregated at the expression stage as previously reported [2].

RESULTS: The recombinantly expressed human βB2-crystallin refolding pathway was investigated in two different temperatures, but no significant differences were found (Fig. 1). Thus, it was suggested that there is no significant effect between 35 °C and 37.5 °C with respect to temperature effects on βB2-crystallin folding *in vivo*. This would be caused by the heat stability of βB2-crystallin itself. Since the mimicking congenital cataracts were not expressed in the soluble fraction at 37.5C, suggesting a possible temperature effect on such mimic.

Fig. 1. The βB2-crystallin folding pathway was observed in the presence of each concentration of urea in different temperature.

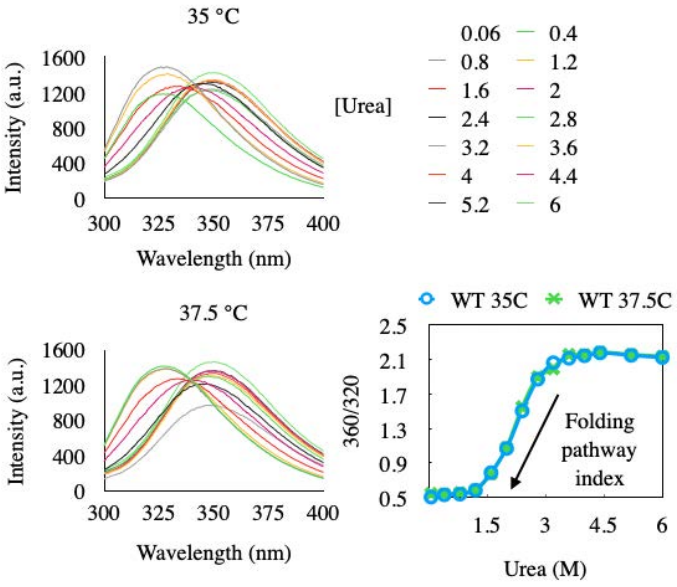

REFERENCES:

[1] N. Yamamoto *et al.*, Cells., **12** (2020) 2670.
[2] W. Zhao *et al.*, J Biol Macromol., **103** (2017) 764–770.

CO6-32

Survey on Radioactive Cesium Migration between Environment and Body of Wild Boar (*Sus scrofa*) Living in Fukushima Prefecture

M. Fukushima[1], Y. Tsuji[1], Y. Iinuma[2], H. Komatsu[3], H. Sugawara[4], S. Mochizuki[4], K. Murakami[3], K. Kanda[3]

[1]*Faculty of Science and Engineering, Ishinomaki Senshu University*
[2]*Research Reactor Institute, Kyoto University*
[3]*Fukushima Prefectual Centre for Environmental Creation*
[4]*Faculty of Food and Agriculture Sciences, Fukushima University*

INTRODUCTION: To study the migration of radioactive cesium caused by Fukushima-Daiichi Reactor accident between environment and several species of wild animals, stable cesium levels in muscles, blood, and livers of wild boars living in Fukushima Pref. were analyzed.

EXPERIMENTS: Wild boars were trapped in Namie, Futaba, Ohkuma, and Katsurao, (inside of Difficult-to-return Zone, n = 25 in total) from May to September 2023, and Nihonmatsu (outside of Difficult-to-return Zone, n = 21) from December 2021 to February 2023 under the permission of Fukushima Pref.. After euthanasia by neck shot, musclus quadriceps, contents of the stomach, blood, and the liver were removed from body, freeze-dried, pulverized, and gamma-ray counting was done for Cs-134 and Cs-137 radioactivity. Also, before freeze-drying, some amount of stomach content was kept in 70% ethanol soln. and separated each materials unter optical microscope for estimating wild boar diet; n = 166 and 40 for wild boars from inside and outside of Difficult-to-return Zone, respectivily. One portion of dried power was supplied for short irradiation in KUR. Eight elements of Ca, Cl, Cu, K, Mg, Mn, Na, and V of wild boar diet were analyzed by the condition of TcPn irradiation, also eight elements of Co, Cr, Cs, Fe, Rb, Sc, Se, and Zn of muscles, blood, and livers were analyzed by irradiation for 1 hour.

RESULTS: **<Radioactive Cs levels in diet, muscles, blood, and livers>** Cesium-137 levels in diet collected from Namie and Nihonmatsu, muscles, blood and livers from inside and outside of Difficullt-to-return Zone are shown in Fig.1. In all samples except diet samples, Cs-137 levels of the samples from inside of Difficult-to-return Zone were 1-2 order higher than those from outside.
<Correation between Cs-137 and stable Cs> Strong correation between Cs-137 and stable Cs in muscles, blood, and livers were found for all three organs, especially organs from Difficult-to return Zone. Correation between Cs-137 and stable Cs is shown in Fig. 2 for livers from Difficult-to-return Zone. This may be thought that Cs-137 in the wild boar diet moves in a same metabolism as stable Cs in the body of wild boars.

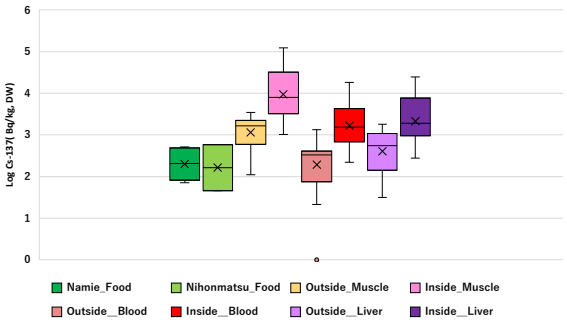

Fig.1 Cs-137 levels in diet, muscles, blood, and livers from inside and outside of Difficult-to return Zone.

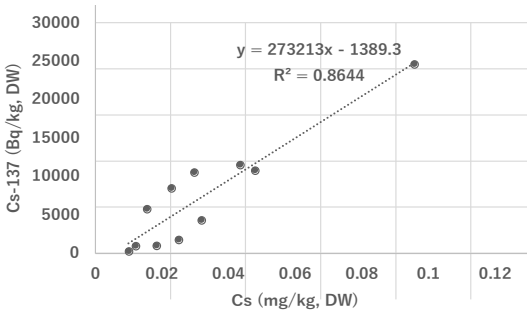

Fig.2 Correation between Cs-137 and stable Cs in livers from Difficult-to return Zone.